

**Study Of Excited Intermediate States In  $p(e, e'K)\Sigma^0$  Reactions**

**K. Assamagan, S. Avery, O. K. Baker, H. Bitao, J. Cha,  
E. Christy, A. Cochran, L. Cole, L. Gan, A. Gasparian,  
P. Guèye(spokesman) , C. Jackson, M. Harvey, W. Hinton,  
C. Keppel, L. Tang, A. Uzzle, L. Yuan**  
Hampton University, USA

**C. Armstrong, R. Carlini, R. David, R. Edwards, R. Ent, A. Lung,  
J. Mitchell, G. Prezeau, W. Vulcan, S. Wallace, S. Wood, C. Yan**  
Thomas Jefferson National Accelerator Facility, USA

**R. Williams**  
University of Wisconsin LaCrosse, USA

**G. Niculescu**  
Ohio University Athens, USA

**I. Niculescu**  
George Washington University, USA

**E. Swanson**  
North Carolina State, USA

**M. Khandaker**  
North State University, USA

**P. Markowitz, J. Reinhold**  
Florida International University, USA

**B. Zeidman**  
Argonne National Laboratory, USA

**T. Angelescu, I. Lazanu, L. Teodorescu**  
Bucharest University, Romania

**A. Margaryan, H. Mkrtchyan, S. Stepanyan, V. Tadevosyan**  
Yerevan Physics Institute, Armenia

**M. Amarian, E. Cisbani, S. Frullani, F. Garibaldi,  
M. Iodice, R. Iommi, G. Urciuoli**  
Instituto Nazionale de Fisica Nucleare-Sanità, Rome, Italy

**R. De Leo, L. Lagamba**  
Instituto Nazionale de Fisica Nucleare-Sanità, Bari, Italy

**S. Danagoulian, A. Ahmidouch**  
North Carolina A&T University, USA

**H. Gao, D. Dutta**  
Massachusetts Institute of Technology, USA

**H. Breuer, C. C. Chang**  
University of Maryland, College Park, USA

(January 24, 2000)

## Jefferson Lab Proposal

### Study Of Excited Intermediate States In $p(e, e'K)\Sigma^0$ Reactions

This proposal describes an experiment to study excited intermediate states in kaon electro-production via the  $\Delta^* \rightarrow K^+\Sigma^0$  decay channel. The physics goals are: investigation of SU(3) violation and information on the transition form factors by measurement of the  $Q^2$  dependence of  $\Delta^*$  resonance decays; test of Regge theory at intermediate energy and experimental signatures of possible missing, molecular or exotic resonances.

The experiment will use unpolarized electron beam in Hall C, using standard equipment: the HMS and SOS detector packages as were used in the kaon electro-production experiments which were completed during the fall of 1996, and the 4 cm liquid hydrogen target.

The  $\Delta^*(1900)$ ,  $\Delta^*(1910)$ , and  $\Delta^*(1920)$  resonances, the candidate pentaquark baryonium system  $X(2000)$ , and possible missing resonances will be studied by looking at the invariant mass  $W$  distribution of the  $\Delta^* \rightarrow p + \pi^0$  and  $p(e, e'K)\Sigma^0$  reactions; the  $\Sigma^0$ -hyperon being selected by missing mass in the  $p(e, e'K)Y$  reaction (where  $Y = \Lambda, \Sigma^0$ ).

By detecting the proton from the  $\Delta^* \rightarrow p + \pi^0$  decay for the same kinematic settings than the  $\Sigma^0$  channel, relative information on the  $g_{\Delta^*K\Sigma^0}$ , and  $g_{\Delta^*p\pi^0}$  coupling constants will be extracted. In addition, a  $Q^2$  dependence will be performed to probe the transition form factors of these resonances produced during the reaction.

The more speculative exotic baryon will be distinguished from background threshold effect processes by looking at its  $Q^2$  dependence: the  $N^*$  and  $\Delta^*$  resonance dominated background is expected to follow a different  $Q^2$  dependence than the  $X$ -baryon.

These measurements will provide unique information on intermediate excited states, missing resonances and on exotic systems in strangeness production. This experiment will be unprecedented for measurements of the  $Q^2$  distribution in the resonance region and evidence of such exotic systems at non zero invariant four-momentum transfer with high precision in the  $\Sigma^0$  channel.

Fifteen (15) days of beam time is requested to cover the necessary invariant mass region for fifteen (15) settings at four-momentum transfers ranging from 0.55 to 1.05 (GeV/c)<sup>2</sup>.

## I. OVERVIEW

With the new generation of high current, high duty factor electron accelerators, it has become possible to study strangeness in photo- and electro-production with an unprecedented level of accuracy. Since it began in 1995, the CEBA machine at the Thomas Jefferson National Accelerator Facility (Jefferson Lab) has proven to be a powerful tool in studying the electromagnetic production of hadronic systems containing a strange constituent quark.

Study of the photo- and electro-production of kaons requires the understanding of several underlying processes in the s-channel which involve direct excitations of the nucleon target. This proposal focuses on electro-production of  $\Sigma^0$ -hyperons off proton targets. The corresponding intermediate excited states on the proton involve  $\Delta^*$  and  $N^*$  resonances, and possibly missing resonances, molecular and/or exotic baryons.

The  $\Delta$ -resonance region has been subject to numerous studies since the discovery of the  $\Delta(1232)$  and its associated excitations in hadron-hadron, photon and electron scattering experiments in both inclusive and exclusive channels [1–4]). Most of the exclusive data were collected by looking at the  $\Delta^* \rightarrow N\pi$  decay. Few experiments studied the  $\Delta^* \rightarrow K\Sigma^0$  channel [5]. The data which involve the electromagnetic probe are scarce and have poor statistics (see a review in [6]).

Recent high precision data on kaon electro-production off proton and deuterium targets at Jefferson Lab [7–11] show that isobar based models which account for excited nucleon states up to spin 3/2 [12] are sufficient to reproduce reasonably well the experimental data at low  $Q^2$  (Figs. 1 and 2).

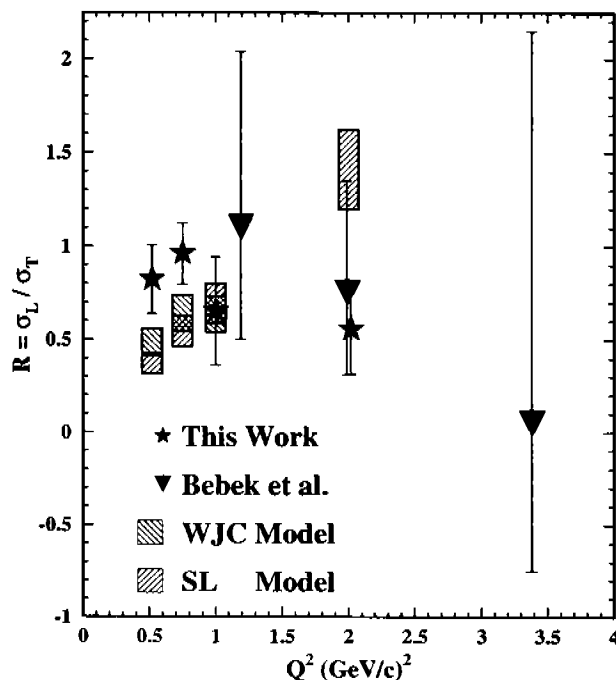


FIG. 1.  $Q^2$  dependence of the  $\Lambda$ , hyperon in kaon electro-production [8].

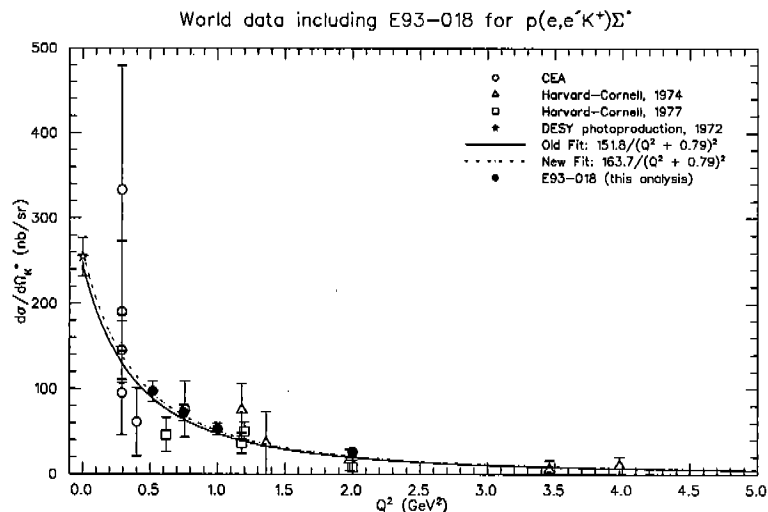


FIG. 2.  $Q^2$  dependence of the  $\Sigma^0$  hyperon in kaon electro-production [9].

There is a great interest in extracting the  $\Delta^*\pi N$  and  $\Delta^*K\Sigma^0$  coupling constants (which are currently not precisely determined [12]), since information on SU(3) violation through the study of the  $\Delta^* \rightarrow K\Sigma^0$  and  $\Delta^* \rightarrow \pi N$  [13] decays can be investigated<sup>1</sup>). An understanding of the properties of the  $\Delta^*$  resonances is an important factor for the comprehension of the reaction mechanism:  $\gamma_v + p \rightarrow \Delta^* \rightarrow K\Sigma^0$ .

It is also believed that at threshold, the K-meson and  $\Sigma^0$ -hyperon could form a lightly bound state, hence a pentaquark exotic baryon. This is not a new idea.

In the late 50s and early 60s the known hadrons were grouped into the Eightfold Way SU(3) families: singlets, octets, and decuplets. In 1964, the Constituent Quark Model (CQM) classified the observed multiplet structures in terms of the quark-antiquark ( $q\bar{q}$ ) composition of mesons and the three-quark ( $qqq$ ) composition of hadrons. In 1965, Nambu [14] proposed the idea of color to explain why this was so: "if quarks came in three colors, then they would tend to bind together in colorless combinations". The simplest colorless objects which can be formed from tri-colored quarks are just  $q\bar{q}$  and  $qqq$ . However, these (minimal) colorless systems are by no means the only colorless multi-quark states which could be constructed. One can put together an infinite variety of more complex combinations:  $qq\bar{q}\bar{q}$ ,  $qqqq\bar{q}$  . . . .

It is now ten years since the proposal of the existence of the pentaquark [15] and suggestions for its search via  $p\phi\pi^-$  decay mode [16]. Despite subsequent experimental progress and analysis of models for pentaquark structure, decay, and signatures [17] there is still no convincing experimental evidence for the existence of the pentaquark nor of any other hadron which cannot be described in a constituent quark model as a  $qqq$  or  $q\bar{q}$  state [18,17].

The possible existence of exotic hadrons remains a principal question in hadron spectroscopy and in the understanding of how the binding of quarks and gluons into hadrons is described by QCD [15]. The first exotic hadron search was for the  $H$  dibaryon [19]. Jaffe's original calculation and subsequent work [20] indicate a gain in hyperfine interaction energy by recoupling color and spins in the six quark system over the two- $\Lambda$  system. However, a lattice gauge calculation [21] indicated the  $H$  to be unbound and well above the  $\Lambda\Lambda$  threshold. The lattice calculation showed a repulsive  $\Lambda\Lambda$  interaction generated by quark exchange [17] which is not included in simple model calculations and could well

<sup>1</sup>This SU(3) study of these two reactions is done in appendix B and the SU(3) violation will be explained later in section II.

prevent the six quarks from coming close enough to feel the additional binding of the short range hyperfine interaction. Such a repulsive exchange force cannot be present in pentaquarks. More recent lattice calculation [22] tends to confirm this result.

From the 60s to the 90s, theoretical as well as experimental interests flourished upon the search of  $qq\bar{q}\bar{q}$  baryoniums and other exotic hadrons [23–26] without success. Recently, experimental claims of new possible exotic states not forbidden by Quantum Chromodynamics (QCD) have been reported by the SPHINX [27,28] collaboration at IHEP. These two states were seen from coherent diffractive scattering of 70 GeV protons off a carbon target in the reactions:

$$p + C = [\Sigma^0 + K^+] + C, \quad (1)$$

$$p + C = [\Sigma^0(1385) + K^+] + C, \quad (2)$$

where the square brackets signify that the signal was seen in the invariant mass spectra of these strange particles. Two structures labeled X(1999) and X(2052) were identified as exotic pentaquark hadrons and could correspond to the elementary two-step process:

$$\gamma_v + p \rightarrow K^*\Sigma^0 \rightarrow X \rightarrow K\Sigma^0. \quad (3)$$

More recently [29], Bennhold *et al.* were able to fit the new data on kaon photo- and electro-production obtained at ELSA [30] and Jefferson Lab [31] by including a missing resonance predicted by the quark model of Roberts and Capstick [32]. A similar result was obtained by Saghai *et al.* and Han *et al.* when including higher spin resonances (up to spin 5/2) and off-shell effects in the elementary process [33,34].

The need for the understanding of the elementary process in the intermediate resonance region is of fundamental interest for the comprehension of the new experimental data obtained in the strangeness sector. Especially in the  $\Sigma^0$  channel, which gives access to the contribution of  $\Delta^*$  resonances and where the data are scarce in comparison to the  $\Lambda$  channel [9].

The possible novel states observed in the SPHINX experiment are easily accessible at Jefferson Lab and have masses which are close to the excited  $\Delta^*$  states which are the primary focus of the experiment described in this document,  $\sqrt{s} \sim 1.9 - 2.2$  GeV. In this proposal, cross section measurements will be performed in the resonance region, and in order to resolve the overlapping resonance contribution to the production amplitudes we will perform a K-matrix analysis of the data.

## II. PHYSICS MOTIVATIONS

### A. $\Delta^*$ resonances

#### 1. Transition form factors

Information in the nucleon resonance region of real and virtual photon-nucleon interactions is still not well understood and information from both theory and experiments is needed. Recently, the momentum distributions of the constituent quarks inside the nucleons and the prominent electro-produced resonances – namely,  $\Delta(1232)$  and  $S_{11}(1535)$  – have been investigated in the two most sophisticated available quark potential models, based respectively on the assumption of the valence + gluon dominance [35] and on the exchange of the pseudo-scalar Goldstone bosons arising from the spontaneous breaking of chiral symmetry [36]. The elastic and transition form factors have been calculated within a relativistic approach formulated on the light-front, adopting a one-body current with constituent quark form factors. The result suggests that soft, non-perturbative effects can play a relevant role for explaining the existing data on elastic as well as transition form factors for  $Q^2 \leq 20$  (GeV/c)<sup>2</sup>.

Experimentally, there has been and still exist an extensive program on studying the intermediate nucleon states especially with the new generation of accelerators (see a review in [1–3,37]). Generally, one performs a partial wave analysis (measurements of the multipole amplitudes) of the data. In photo-production experiments this method gives information on the relative phases and absolute value of the partial waves amplitudes which depend on the photon energy and the relative angle between the kaon and the photon. In electro-production experiments there is an additional dependence on  $Q^2$ , and hence a sensitivity to the transition form factors (see appendix A). This is presently the most commonly used approach in analyzing experimental data if one wants to extract the partial waves of the resonances involved in the reaction mechanism.

Another approach consists of the K-matrix analysis of the data. The basis of this method is the Bethe-Salpeter equation. Largely used in hadron-hadron reactions, this method has recently been adapted to photon induced reaction [38]. In the K-matrix approximation, the coupled channel Bethe-Salpeter equations

$$K = V + V\mathcal{R}e(G_{BS})K, \quad (4)$$

$$T = K - iK\mathcal{I}m(G_{BS})T, \quad (5)$$

reduce to the relation

$$T = \frac{V}{1 - iV}, \quad (6)$$

when setting  $K = V$ .  $G_{BS}$  is the Bethe-Salpeter propagator,  $V$  the potential and  $T$  the T-matrix of the interaction.

Besides Hermiticity, no further constraints on the potential  $V$  are needed. This potential is constructed from effective Lagrangians and describes the couplings between all involved particles. The corresponding model is unitary and includes a large number of reaction channels:  $\pi N \rightarrow \pi N$ ,  $\pi N \rightarrow \pi\pi N$ ,  $\pi N \rightarrow \eta N$ ,  $\pi N \rightarrow K\Lambda$ ,  $\pi N \rightarrow K\Sigma \dots$

The K-matrix formalism has been applied to obtain the effective coupling constants<sup>2</sup>, masses and

---

<sup>2</sup>The effective coupling constant is define here as the product  $g.F(q^2)$ , where  $g$  is the bare coupling constant and  $F(q^2)$  the form factor.

decay widths of several states from various reaction channels involving meson-nucleon and photon-nucleon interactions [38]. The results are consistent with modest SU(3) breaking.

Also, as pointed out by Mukhopadhyay [39], the spectroscopy of excited baryons is a powerful tool to study QCD. In fact, the study of excitations and propagation of delta isobars in nuclear media provides the first scale of relevance to QCD, that set by the color magnetic interaction (CMI). Its largeness, compared to nuclear binding energy per baryon, is the reason why a nucleus is made mostly of nucleons, and not of excited baryons. Color magnetic forces can be understood as the non-Abelian analogue of ordinary magnetic interaction [40]: the short-range quark-quark interaction, derivable from the underlying renormalizable gauge theory (QCD) may be taken to be Coulomb-like, with effective short-range force arising from the one-gluon exchange. This contains among other terms the color magnetic hyperfine interaction.

At the present time, only few measurements exist in kaon photo- (with only 5 angles) and electro-production of kaons for the  $\Sigma^0$  channel [9–12]. New data from SAPHIR [30] and CLAS [41] are expected to be available soon and will provide additional information.

Extraction of the properties on  $\Delta^*$  in kaon electro-production with high accuracy will provide important information on the understanding of the intermediate states involved in the elementary  $\gamma vp \rightarrow K\Sigma^0$  reaction mechanism and will serve as an additional constraint in existing K-matrix based models. The measurements perform with the proposed experiment will provide high quality  $Q^2$  dependence data for  $\Sigma^0$  production in the resonance region from threshold up to about 2.15 GeV.

## 2. SU(3) violation

In the SU(3) scheme, the reactions:

$$\Delta^* \rightarrow \pi N, \quad (7)$$

$$\Delta^* \rightarrow K\Sigma, \quad (8)$$

are characterized by  $|g_{\Delta^*\pi N}| = |g_{\Delta^*K\Sigma}|$  (see appendix B). Using a simple non-relativistic QCD based model, Isgur [13] shows that the ratio  $g_{\Delta^*\pi N}/g_{\Delta^*K\Sigma}$  can be very distorted (far from unity) near threshold production. This result is attributed to color interactions between quarks.

As pointed out in [13], the  $\Delta^* \rightarrow K^+\Sigma^0$  channel is one of the most suitable channels to study this type of SU(3) violation since it allows strong constraints on the parameters of the hadron-hadron potential. However, in order to obtain precise information on such type of violation, one should perform a parallel study of both  $\Delta^* \rightarrow \pi N$  and  $\Delta^* \rightarrow K^+\Sigma^0$  decays. The comparison of the corresponding cross section productions is a direct measurement of the relative discrepancy between the coupling constants. In fact, the matrix elements for the reactions in (7) and (8) are proportional to the effective Lagrangians:

$$\mathcal{L}_\Delta^1 = \mathcal{L}_{\Delta^* \rightarrow \pi N}, \quad (9)$$

$$\mathcal{L}_\Delta^2 = \mathcal{L}_{\Delta^* \rightarrow K\Sigma}, \quad (10)$$

where  $\mathcal{L}_{\Delta^* \rightarrow \pi N} \propto g_{\Delta^*\pi N}$  and  $\mathcal{L}_{\Delta^* \rightarrow K\Sigma} \propto g_{\Delta^*K\Sigma}$ . This type of experiment has never been done yet.

Experimental data on the  $\Delta^*$  resonances near threshold will give a better understanding on the  $g_{\Delta^*\pi N}/g_{\Delta^*K\Sigma}$  ratio, which will allow a test of possible SU(3) violation. The data provided from the proposed experiment will be analysed via a coupled-channel based approach, allowing information on the individual quantum numbers, relative phases and coupling constants of the  $\Delta^*$  involved in the process.

## B. Exotic baryons and missing resonances

### 1. QCD and Regge models

The most probable configurations of  $qqqq\bar{q}$  stable states are  $(qqq)-(q\bar{q})$  where both clusters form a color octet (octet-bonded state), and  $(qq)-(qq\bar{q})$  in the color  $6-\bar{6}$  representations (sextet-bonded states) [42,43]. The latter is much less stable because the color triplet  $qq\bar{q}$  subsystem always contains a  $q\bar{q}$  pair which is a color singlet. As this pair does not feel the confinement forces, the  $qqqq\bar{q}$  system would easily dissociate into a colorless baryon ( $qqq$ ) system and a meson.

Let  $qqq \equiv \Theta$  and  $q\bar{q} \equiv D$ . If  $\Theta$  and  $D$  are separately color singlets, they will interact only via the Van der Waals forces of QCD and will dissociate rapidly into a baryon and a meson. However, if the system  $\Theta D$  is a color singlet with  $\Theta$  and  $D$  being separately color octets and with large non-zero relative angular momentum  $L$ , this system should be linked by very strong forces and will have enhanced stability (i.e., long lifetime compared to a usual hadronic resonance state): the anti-quark in  $D$  is prevented by a centrifugal barrier from tunneling into  $\Theta$  where it can combine with a quark in  $\Theta$  to make a (colorless) meson. The same would be true for a color sextet  $qq$  group bound to a color sextet  $qq\bar{q}$  system. Additional stability is anticipated if  $\Theta = qqs$  and  $D = q\bar{s}$  clusters contain strange quarks since their decay to open non-strange ( $\pi, \rho, \omega$ ) channels should be OZI suppressed.

The multi-quark state of mass  $M_L$  with angular momentum  $L$  between the two groups of quarks is assumed to fall on Regge trajectories where the slope is dependent on the color  $C$  of the two individual quark groups:

$$L = \alpha_0 + \alpha'_C M_L^2. \quad (11)$$

In the MIT bag model [44], Johnson and Thorn [45] have shown that this formula includes all contributions of the color field to the energy of the system when we neglect the spin of the quarks. They also calculate  $\alpha'_C$  and find it to be inversely proportional to  $\sqrt{K}$ , where  $K$  is the value of the quadratic Casimir operator for color  $C$ . This gives:

$$\alpha'_8 = \frac{2}{3}\alpha'_3, \quad (12)$$

$$\alpha'_6 = \sqrt{\frac{2}{5}}\alpha'_3, \quad (13)$$

$$\alpha'_3 = 0.9 \text{ (GeV}/c^2\text{)}. \quad (14)$$

One identified state of the type  $\Theta D$  will fix the parameter  $\alpha_0$  of the Regge formula (11). The ground state of the  $qqqq\bar{q}$  system should occur when all quarks are in relative s-wave (the  $\Theta$  and  $D$  clusters are in a relative p-wave) and the decoupling from pionic decay channels is OZI suppressed (hence  $\Theta$  and  $D$  should carry strangeness).

Recently, a theoretical calculation based on a Regge framework which implements unitarity by *Reggeizing* a gauge invariant combination of Born diagrams has been developed [46]. These two improvements with respect to conventional isobar models were shown to be an essential feature to explain numerous characteristics of photo- and electro-production data for both pions and kaons [46,47]:  $\pi^+/\pi^-$  ratios, momentum and energy variation of the differential cross sections ... This model reproduces the ratio (decreasing at large  $Q^2$  [8]) between the longitudinal and the transverse cross sections of kaon electro-production recently determined at Jefferson Lab [31]. This surprising result seems to indicate a wider application of the Regge theory down to the intermediate energy level (this theory is believed to work only in the high energy regime  $W \geq 3$  GeV).

Experimental existence of exotic pentaquark baryons could reinforce the prediction of the well-established gauge field theory of the strong interaction (QCD) and could play a major role in the constraint of Regge-type models in the intermediate energy regime. The confirmation or not of the states seen in the SPHINX experiment is easily feasible with the precision currently achieved with the Hall C experimental spectrometer setup. The  $W$  distribution covered by the experiment proposed in this document will include these states and should allow to make a definite conclusion on their possible existence.

## 2. Molecular Model

Another possible interpretation of the claimed pentaquark systems is that these states are molecular states of strange particles. The  $a_0/f_0(980)$  states are established examples [48] of states that find their most natural interpretation as molecular states, having their wave functions with large components of lightly bound  $K\bar{K}$  mesons (see [49] for other molecular-type systems). This interpretation is a direct consequence of the Van der Waals nature of the potential which is usually found in atomic and molecular physics.

In the particular case of the  $\gamma np \rightarrow K\Sigma^0$  reaction, a  $K^*(892)$  could couple to the  $\Sigma^0(1193)$  and form a state with a mass comparable with  $X(2085)$ . In addition, the sum of the widths of the  $K^*$  (51 MeV) and the  $\Sigma^0$  (lifetime of  $7.4 \times 10^{-20}$  s), is comparable to the one claimed by the SPHINX collaboration [27].

If the X-baryons do couple to the  $K - \Sigma$  channel, it will be important to distinguish their exotic versus molecular structure, as well as identify their quantum numbers. The measurements performed will provide basics for the understanding of the dynamics of these states.

## C. Isobar, Quark, hybrid and Lattice models

### 1. Isobar models

From the new  $\Lambda$  photo-production SAPHIR data [30], isobaric based models have been recently reconsidered by incorporating higher spin resonances [33,34] and missing resonances [29]. Previous conventional isobaric models include up to spin 3/2 resonances in the s and u channels. Although the overall trend of the various distributions obtained were reasonably well reproduced for the low ( $Q^2, W$ ) region, a divergence behavior from the data is observed when going towards the higher ( $Q^2, W$ ) region. In order to reproduce the new experimental results in this kinematic regime, addition of higher spin resonances and off-shell effects in the elementary process seem to be necessary features for isobaric models. This work was recently done by [33] and [34]. On the other hand, guided by the coupled-channel analysis of [38], Bennhold *et al.* include, in the low-energy resonance part of their model, three states that have been found to have significant decay widths into the  $K^+\Lambda$  channel, namely the  $S_{11}(1650)$ ,  $P_{11}(1710)$ , and  $P_{13}(1720)$  resonances. A structure around 1900 MeV was attributed to the  $D_{13}(1895)$  missing resonance predicted by the relativistic quark model of Roberts and Capstick [32] which is expected to have a significant  $\gamma N$  and  $K\Lambda$  branching ratios. It is evident that more high quality data are needed in this energy range to disentangle between these various models. Modifications to the  $\Sigma^0$  channel is being developed by [33] which will have implications on the possible features observed in the SAPHIR data around  $W = 2$  GeV.

## 2. Quark Born Diagram formalism

A recent model which describes kaon-nucleon scattering has been developed by T. Barnes and E. Swanson [50]. The KN amplitude is derived in a quark Born diagram formalism where the scattering is taken as a single interaction (one gluon exchange - OGE - spin-spin term) followed by quark line arrangement. In their paper, the authors discuss the importance of KN scattering for extracting information on (i) the origins of non-resonant nuclear forces in a system distinct from NN, (ii) nuclear structure physics (using kaons as a weakly interacting probe), and (iii) searches for possible exotic  $Z^*$  baryon resonances which couple directly to KN. This latter state has a  $q\bar{s}$  structure (with  $q=u$  or  $d$ ) and was predicted by the quark model [51]. A modification of this model is being done for predictions on the quantum numbers and properties of the pentaquark X resonance [52].

## 3. Resonance-Regge hybrid model

As mentioned previously, Regge theory seems to be applicable over a wider range than expected, down to the intermediate energy level [31]. The recent data from ELSA on eta photo-production has led the authors developing a hybrid resonance-Regge formalism which extends the Regge theory to low energy by coupling some known resonances through relativistic Breit Wigner shapes to their former model [53]. This hybrid model is being modified to implement the pentaquark X resonance.

## 4. Lattice QCD

The lattice approach to QCD provides the only known truly non-perturbative regularization scheme. Lattice QCD is believed to be a first principles approach: no parameters apart from those that are inherent to QCD, i.e., the  $n$  quark masses. In order to fit these  $n$  parameters,  $n$  low energy quantities are matched to their experimental values: the lattice spacing  $a(g)$ , that results from a given value of the bare lattice coupling  $g$ , can be obtained by fixing the rho meson mass  $m_\rho$  as determined on the Lattice to the experimental value. The lattice parameters that correspond to physical quark masses  $m_u \approx m_d$  can then be obtained by adjusting  $m_\pi/m_\rho$ ,  $m_s$  from  $m_K/m_\rho$  or  $m_\phi/m_\rho$  ... Once the quark masses have been set and the scale being determined, everything else becomes a prediction. The Jefferson Lab Lattice collaboration group has a primary focus on multi-hadrons system and hadron-hadron interactions [54]. The work involves study of  $N^*$ ,  $\Delta^*$ , ... and form factors. Prediction of their hadron spectrum will be compared to the  $\Delta^*$  and possible experimentally missing resonances obtained from the experiment described in this document.

### III. EXPERIMENTAL STATUS

#### A. $\Delta^*$ resonances

Out of all the  $\Delta^*$  resonances listed in the Particle Data Book [55], only three resonances can potentially be studied in our kinematical regime through kaon electro-production (Table I):  $\Delta^*(1900)$ ,  $\Delta^*(1910)$ , and  $\Delta^*(1920)$ .

| Baryon   | Mass<br>(MeV) | Width<br>(MeV) | I   | J   | P | $\Gamma_{\Delta^* \rightarrow K\Sigma}$ | Knowledge in<br>K $\Sigma$ channel |
|----------|---------------|----------------|-----|-----|---|---|------------------------------------|
| $S_{31}$ | 1900          | 200            | 3/2 | 1/2 | - | 5-10%                                   | very poor                          |
| $P_{31}$ | 1910          | 250            | 3/2 | 1/2 | + | 15-30%                                  | very poor                          |
| $P_{33}$ | 1920          | 200            | 3/2 | 3/2 | + | 5-20%                                   | very poor                          |

TABLE I. Masses, widths, quantum numbers and branching ratio for the  $\Delta^* \rightarrow K\Sigma$  decay mode of the three  $\Delta^*$  resonances proposed to be studied in the experiment described in this document:  $\Delta^*(1900)$ ,  $\Delta^*(1910)$ , and  $\Delta^*(1920)$ .

The other resonances either have no phase-space for this decay, have a too low branching ratio or have a too large decay width ( $\geq 300$  MeV) to be observed in the experiment described in this document.

The Particle Data Book gives up to four stars for these three resonances when studied in  $\pi N$  decay channels. However, as can be seen in the last column of Table I, there is a very poor degree of knowledge in the strangeness production  $\Delta^* \rightarrow K\Sigma$  decay channel.

#### B. Exotic baryons

##### 1. The SPHINX experiment

A wide program studying diffractive hadron production by protons and searching for exotic baryons in these processes is being carried out by the SPHINX collaboration at IHEP [27]. Studies of several proton induced reactions such as  $p + N \rightarrow Y^0 K^+ + N$ ,  $p + N \rightarrow p K^+ K^- + N$ ,  $p + N \rightarrow p p \bar{p} + N$ ,  $p + N \rightarrow p \pi^+ \pi^- \pi^0 + N \dots$  are being done.

Recent experimental data on  $p + C \rightarrow [Y^0 K^+] + C$ , where  $Y = \Sigma^0, \Sigma^*(1385)$  were obtained [27,28] with a 70 GeV incident proton beam on a polyethylene target. From these diffractive production reactions, evidence for new baryon states were claimed in the study of hyperon-kaon effective missing mass spectra (Table II and Fig 3).

| Baryon  | Mass<br>(MeV) | Width<br>(MeV)   |
|---------|---------------|------------------|
| X(1999) | $1999 \pm 6$  | $91 \pm 17$      |
| X(2052) | $2052 \pm 6$  | $35^{+22}_{-35}$ |

TABLE II. Masses and widths of the crypto-exotic pentaquark baryons seen in the SPHINX experiment.

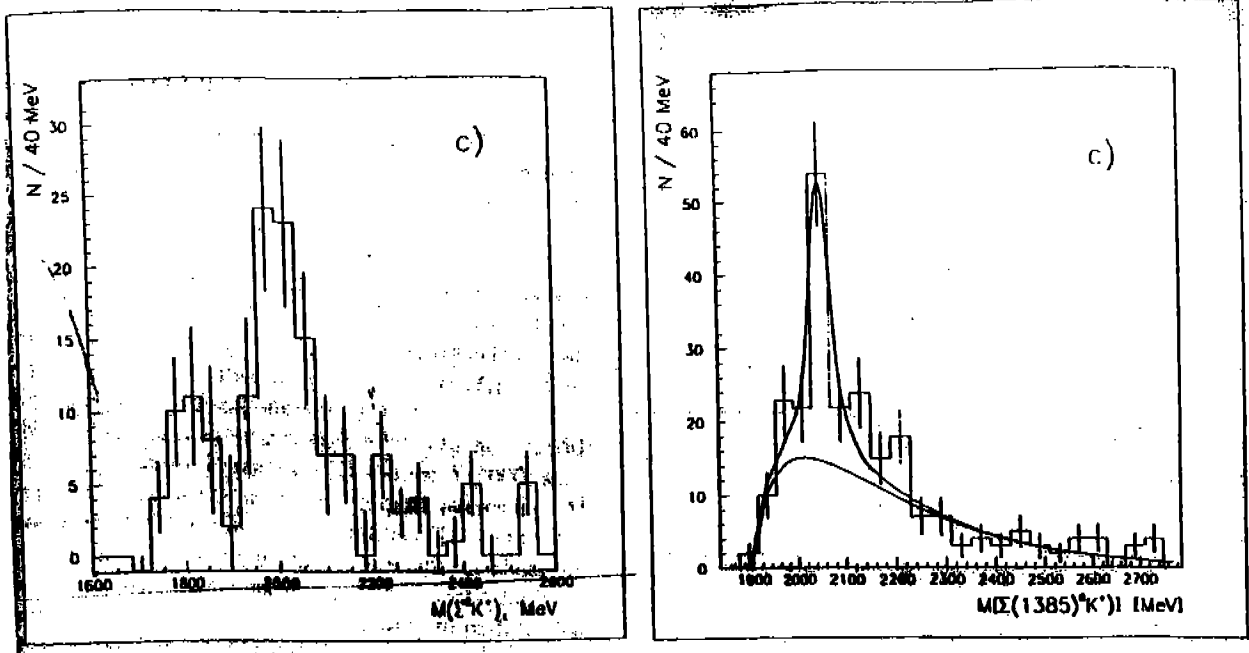


FIG. 3.  $[\Sigma^0 K^+]$  (left) and  $[\Sigma^0(1385)K^+]$  (right) missing masses in the SPHINX experiment.

The unusual features of these massive states, such as small decay widths and anomalously large branching ratios for decays with strange particle emission, were taken to be serious candidates for crypto-exotic pentaquark baryons with hidden strangeness.

### C. The SAPHIR experiment

New kaon photo-production data  $p(\gamma, K)Y$  with  $Y = \Lambda, \Sigma$  were recently taken with the SAPHIR spectrometer at the ELSA accelerator in Bonn [30]. Total cross sections were measured for a wide range of center of mass energy  $W$  which covers the region of interest discussed in this document:  $1.6 < W(\text{GeV}) < 2.15$  (Fig. 4).

In the  $\Lambda$  production data, no enhancement can be seen near 1.999 GeV but one exists at about 2.052 GeV. In the  $\Sigma^0$  channel the data seem to indicate signals appearing at about 1.999 GeV and at about 2.052 GeV, respectively. These results seem to indicate that the observed enhancement at 2.052 GeV seen in both channels could be attributed to threshold effects from coupled channels feeding into the  $K - \Sigma^0$  channel as  $W$  sweeps through the  $K^* - \Sigma^0$ ,  $K - \Sigma^*$  or possible other thresholds. However, the other signal at about 1.999 GeV could be an indication of the existence of a bound state resonance structure.

Using the model described in appendix A and including a final state interaction coupling for the two X-resonances using relativistic Breit-Wigner shapes, we were able to reproduce the two signals which appear at 1.999 GeV and 2.052 GeV, respectively. The solid line in Fig. 4 corresponds to the case where one assumes a coupling to spin  $1/2^+$  resonances only, the dashed line is for the case with coupling to resonances with spin  $1/2^-$  only, and the dot-dashed line is where no crypto-exotic resonance is assumed. The *norm.* factors correspond to normalization factors used to re-scale the model differential cross section to the total cross section. The  $g_{X1, X2}$  are the corresponding coupling constants for both resonances where the numbers outside (inside) the parenthesis correspond to the solid (dashed) line.

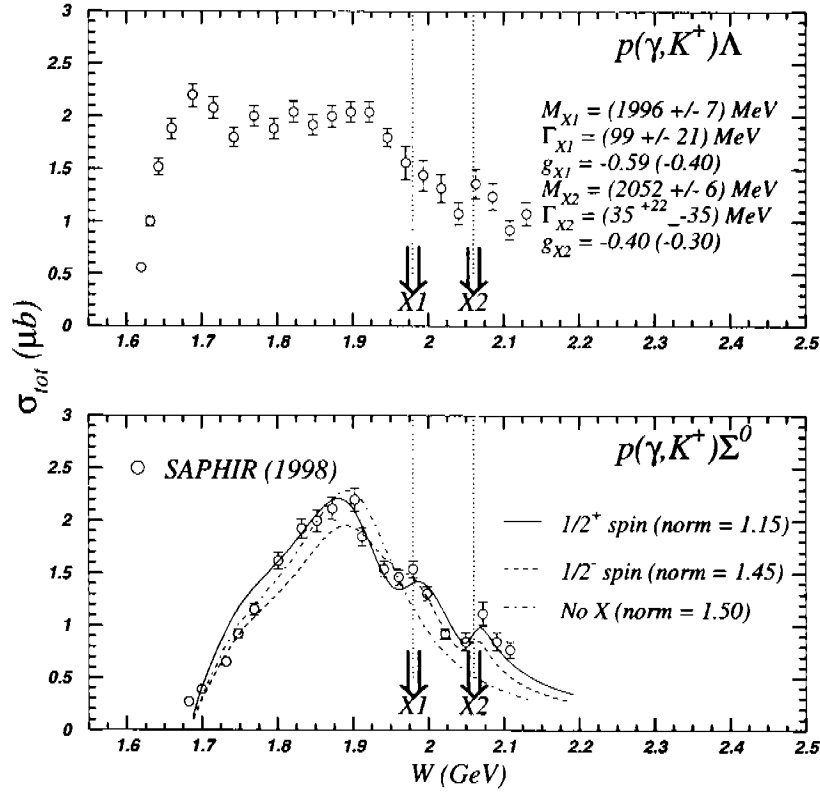


FIG. 4.  $\Lambda$  (top) and  $\Sigma^0$  (bottom) invariant mass distributions in photo-production from [30] and [41] compared to the model prediction described in A: the crypto-exotic baryon X couples to spin  $1/2^+$  resonances (solid), to spin  $1/2^-$  resonances (dashed) and without X (dot-dashed). The vertical (dot) lines show the location of the two predicted X resonances.

One of the intermediate states seen in the SAPHIR experiment, X(1999), could be interpreted as a result of non-threshold effects. This may indicate an isospin  $3/2$  for the state since it is not seen in the  $\Lambda$  channel. Our toy model also seems to indicate a positive parity of the state which can be understood as:  $P_X = P_K \otimes P_{\Sigma^0} \otimes (-1)^{\Delta l} = -1 \otimes 1 \otimes -1 = +1$ , where  $\Delta l$  has been taken to be 1 (as a reminder, the two clusters have to be separated by at least one unit of angular momentum). If the existence of the two states is confirmed experimentally, one can think of them as two degenerate states with a mass of about 2.000 GeV, and the apparent observation of two different masses could be a result of spin-orbit, or color hyperfine interactions (or a combination of the listing degeneracy) between the colored  $K^+$  and  $\Sigma^0$  clusters coupled to different  $J^\pi$ .

#### D. The CLAS experiment

In addition to the experiment performed at SAPHIR, new kaon photo-production data for the same reaction mechanism –  $p(\gamma, K)Y$  with  $Y = \Lambda, \Sigma$  – were obtained with the CLAS detector at Jefferson Lab [41]. Total cross sections were measured for a wider center of mass energy range:  $1.6 < W(\text{GeV}) < 2.35$ . The preliminary analysis of the CLAS data points do not forbid the existence of narrow resonances.

One should not forget that these data sets were extracted from the (almost)  $4\pi$  acceptance of the CLAS and SAPHIR detectors. The trade-off with such large acceptance detectors is that the total number of counts reconstructed fall over the entire acceptance of the detector and one usually extracts the total cross section by averaging over a wide range in  $Q^2$  (for electro-production) and  $t$ . The differential cross section can also (in principle) be extracted from the data. However, one will have to suffer from low statistics. Hence, part of the physics can be washed out and, in the case of very narrow resonances with low production cross section (which is the case for the X-baryon and seems to be on the order of a few % of the hyperon production), the binning of the data may mask possible enhancements. In Hall C, one will not suffer from these issues discussed above since a dedicated coincidence experiment (where two particles are detected in the final state) not only focusses on a small acceptance of the phase space, but also recent data on kaon electro-production [2,9] shown missing mass resolution on the order of 4-6 MeV (FWHM), suitable to search for such type of narrow resonances.

## IV. PROPOSED EXPERIMENT

### A. Method

In this experiment, we propose to investigate the following processes:

$$\gamma_\nu + p \rightarrow \Delta^* \rightarrow p + \pi^0, \quad (15)$$

$$\gamma_\nu + p \rightarrow \Delta^* \rightarrow \Sigma^0 + K^+, \quad (16)$$

$$\gamma_\nu + p \rightarrow \Sigma^0 K^+ \rightarrow X \rightarrow \Sigma^0 K^+. \quad (17)$$

The scattered electrons will be detected in the High Momentum Spectrometer (HMS) and the electro-produced protons and kaons in the Short Orbit Spectrometer (SOS). The missing mass spectrum of the  $\pi^0$  and  $\Sigma^0$  will be reconstructed. In the case of the  $\Sigma^0$ , the  $\Lambda$  hyperon which is also produced during the reaction will be separated using standard missing mass techniques as in the previous kaon electro-production experiments [56,57] (see section IV E). From the  $\pi^0$  and  $\Sigma^0$  samples the invariant mass distributions for all processes listed in 15-17 will be extracted for different  $Q^2$  values ranging from 0.45 to 1.05 (GeV/c)<sup>2</sup>.

*a.  $\Delta^*$  baryons:* The ratio of the rates  $R_i$  between  $\pi^0$  and  $\Sigma^0$  production will be used to study the SU(3) violation. In first order, this ratio is proportional to the ratio of the coupling constants (appendix B):

$$\frac{R_{\pi^0}}{R_{\Sigma^0}} = \left( \frac{g_{\Delta^* p \pi^0}}{g_{\Delta^* K^+ \Sigma^0}} \right)^2. \quad (18)$$

In the overlapping resonance region, there will be contributions from many other resonances than the one studied in the proposal. We will make use of a K-matrix coupled-channel based analysis which includes all known resonances up to the energy range measured to be able to extract information on the  $\Delta^*$ .

First, since the  $N^*$  contribute in both  $\Sigma^0$  and  $\Lambda$  channels, and that both hyperons will fall within the SOS acceptance simultaneously, information on all  $N^*$  contributing in these processes will be measured<sup>3</sup>. Feeding the  $Q^2$  dependence of both channels in a coupled-channel based model analysis will allow extraction of the  $\Delta^*$  information: the individual quantum numbers and relative phases of the  $N^*$  could be extracted<sup>4</sup>, and the coupling constants of interest.

Second, the simultaneous measurements of the three productions  $K^+ \Sigma^0$ ,  $K^+ \Lambda$ , and  $\pi N$  at various  $Q^2$  will be used in the same way to obtain information on SU(3) violation.

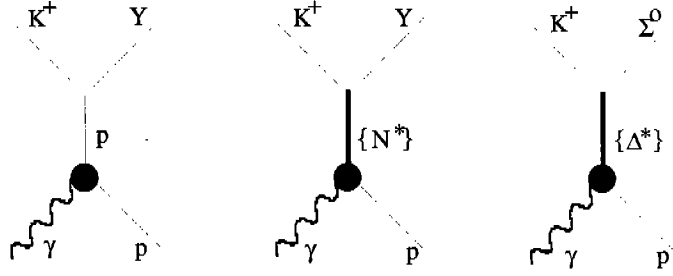
*b. Exotic baryon:* In the particular case of the X(2000), because the elementary reaction mechanism involves several other background processes (Fig. 5), one has to be able to separate this state from the underlying background.

---

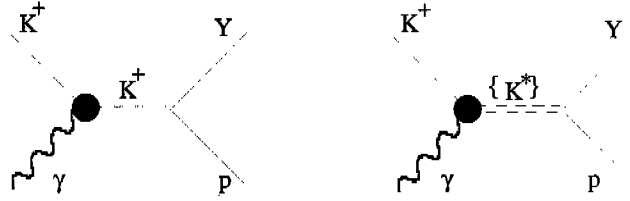
<sup>3</sup>The  $N^*$  contribute in both channels while the  $\Delta^*$  contribute only in the  $\Sigma^0$  channel.

<sup>4</sup>Since the model allows couplings of various channels, the interferences between all resonances are also taken into account.

s- channel graphs:



t- channel graphs:



u- channel graphs:

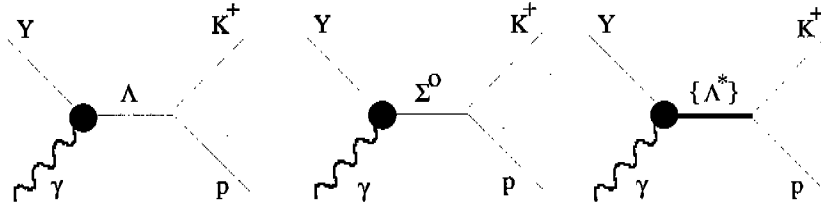


FIG. 5. Feynman diagrams for kaon electro-production.

The background processes result from proton-baryon interactions which excite  $qqq$  systems. The corresponding  $Q^2$ -dependence should follow a different behavior than the pentaquark  $X(2000)$ . Therefore, one could disentangle between the two by performing a  $Q^2$  dependence of the ratio of the possible enhancements to the underlying background distribution. In addition, a  $K$ -matrix analysis will be performed to extract information on the quantum numbers of this state.

For cross-calibration, we will make use of some kinematic settings which were taken during the E93-018 experiment [56] where differential cross sections for the  $p(e, e'K)\Sigma^0$  channel were measured for  $W \leq 1.84$  GeV. Three kinematic points [ $W=1.84$  GeV,  $Q^2 = 0.52$  (GeV/c) $^2$ ], [ $W=1.84$  GeV,  $Q^2 = 0.75$  (GeV/c) $^2$ ], and [ $W=1.81$  GeV,  $Q^2 = 1.00$  (GeV/c) $^2$ ] will be taken with the same spectrometer settings as in [56].

## B. Kinematics

The proposed kinematic settings to study the three  $\Delta^*$  resonances, possible missing resonances and the crypto-exotic pentaquark baryon  $X(2000)$  in the  $(e, e'K)\Sigma^0$  reaction are displayed in Table III. Fifteen  $Q^2$  points are necessary to extract information on the transition form factors of the  $\Delta^*$ ,

identify a signal for the expected missing and X resonance (see section IV F), and extract information on the dynamics of these particles.

| Kine. | $Q^2$<br>(GeV/c) <sup>2</sup> | W<br>(GeV) | $E_{\text{beam}}$<br>(GeV) | $P_{e'}$<br>(GeV/c) | $\theta_{e'}$<br>(Degrees) | $P_{K^+}$<br>(GeV/c) | $\theta_{K^+}$<br>(Degrees) | $P_p$<br>(GeV/c) |
|-------|-------------------------------|------------|----------------------------|---------------------|----------------------------|----------------------|-----------------------------|------------------|
| 1     | 0.52                          | 1.840      | 4.045                      | 2.433               | 13.20                      | 1.126                | 18.33                       | 0.205            |
| 2     | 0.75                          | 1.832      | 4.045                      | 2.326               | 16.23                      | 1.104                | 19.74                       | 0.508            |
| 3     | 1.00                          | 1.810      | 4.045                      | 2.236               | 19.14                      | 1.216                | 20.78                       | 0.315            |
| 4     | 0.55                          | 1.901      | 4.045                      | 2.295               | 13.98                      | 1.218                | 16.96                       | 0.270            |
| 5     | 0.65                          | 1.900      | 4.045                      | 2.244               | 15.38                      | 1.252                | 17.55                       | 0.288            |
| 6     | 0.75                          | 1.900      | 4.045                      | 2.190               | 16.73                      | 1.289                | 17.94                       | 0.307            |
| 7     | 0.85                          | 1.900      | 4.045                      | 2.137               | 18.04                      | 1.323                | 18.20                       | 0.248            |
| 8     | 0.95                          | 1.901      | 4.045                      | 2.083               | 19.33                      | 1.360                | 18.35                       | 0.272            |
| 9     | 1.05                          | 1.901      | 4.045                      | 2.030               | 20.60                      | 1.395                | 18.42                       | 0.296            |
| 10    | 0.55                          | 2.001      | 4.045                      | 2.088               | 14.66                      | 1.468                | 14.63                       | 0.153            |
| 11    | 0.65                          | 2.000      | 4.045                      | 2.036               | 16.15                      | 1.506                | 15.17                       | 0.177            |
| 12    | 0.75                          | 2.000      | 4.045                      | 1.983               | 17.59                      | 1.545                | 15.54                       | 0.200            |
| 13    | 0.85                          | 2.000      | 4.045                      | 1.929               | 19.00                      | 1.585                | 15.78                       | 0.245            |
| 14    | 0.95                          | 2.000      | 4.045                      | 1.876               | 20.38                      | 1.621                | 15.95                       | 0.245            |
| 15    | 1.05                          | 2.000      | 4.045                      | 1.822               | 21.76                      | 1.661                | 16.01                       | 0.266            |

TABLE III. Proposed kinematic settings. The kinematic points 1, 2 and 3 correspond to the calibration points (same settings as E93-018 [56]). The  $\Delta^*$  kinematics are from 4 to 9, and the exotic baryon kinematics from 10 to 15.

The SOS spectrometer has already been calibrated for momenta down to about 200 MeV from previous pion-electroproduction experiments. A detailed study of the mapping of the SOS magnet was performed in order to investigate saturation effects. It was found that above 100 MeV, the behavior of the magnet was adequate. This is about 150 MeV below our lowest momentum (point 7, Table III).

### C. Experimental setup

In the experiment described in this document, an unpolarized electron beam of  $30 \mu\text{A}$  (or whatever maximum available current below  $100 \mu\text{A}$ ) will impinge on the 4 cm liquid hydrogen target. The scattered electrons will be detected in the HMS in coincidence with the electro-produced kaons which will be identified by the SOS. The standard Hall C equipment will be used in the same configuration as the earlier kaon electro-production experiments [56,57].

### D. The Hall C spectrometers

A detailed description of the Hall C spectrometers can be found in [58]. A schematic view of these spectrometers is shown in Fig. 6 and their typical momentum and angular acceptances in Table IV. Both spectrometers have a solid angle acceptance of about 7 msr.

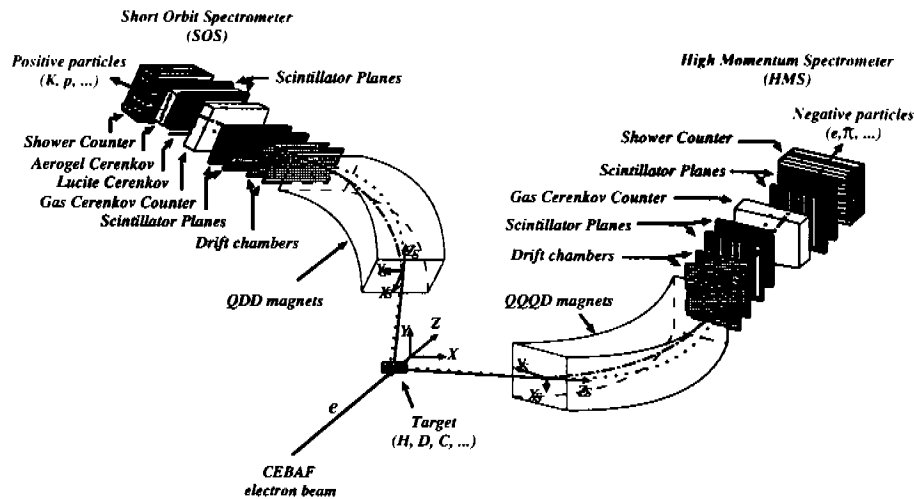


FIG. 6. Schematic view of the detector package of the High Momentum Spectrometer (HMS) and the Short Orbit Spectrometer (SOS) in the experimental Hall C at Jefferson Lab.

|                 | HMS                   | SOS                   |
|-----------------|-----------------------|-----------------------|
| $\Delta P$      | $\pm 7.5\%$           | $\pm 15\%$            |
| $\Delta \Theta$ | $\pm 30 \text{ mrad}$ | $\pm 58 \text{ mrad}$ |
| $\Phi$          | $\pm 70 \text{ mrad}$ | $\pm 38 \text{ mrad}$ |

TABLE IV. The typical angular and momentum acceptances of the HMS and SOS Hall C magnetic spectrometers.

The High Momentum Spectrometer (HMS) will be used as the electron arm and the Short Orbit Spectrometer (SOS) as the hadron (kaon and proton) arm.

The HMS spectrometer consists of a superconducting QQQD system. It will be used in the point-to-point focussing (as was used during the previous kaon experiments). The SOS spectrometer is a water-cooled QDD system and will also be used in its point-to-point tune.

As shown in Fig. 6, both spectrometers are equipped with similar detector packages: two planes of drift chambers, two sets of hodoscope scintillators, a gas Čerenkov and a lead glass shower counter. In addition, an aerogel Čerenkov will be part of the SOS detector system.

The drift chambers will provide tracking information. The hodoscopes will give information on both time-of-flight and  $dE/dx$ . The gas Čerenkov and lead glass shower counters will be used for  $\pi^-/e^-$  and  $\pi^+/e^+$  discrimination, and the aerogel for  $K^+/\pi^+$  discrimination.

During the previous kaon experiments [8,9], separations of 500/1 for  $e/\pi$  and 1000/1 for  $K^+/\pi^+$  were achieved. A typical coincidence time spectrum is displayed in Fig. 7: the central peak at 0 ns corresponds to the identified true coincident kaons.

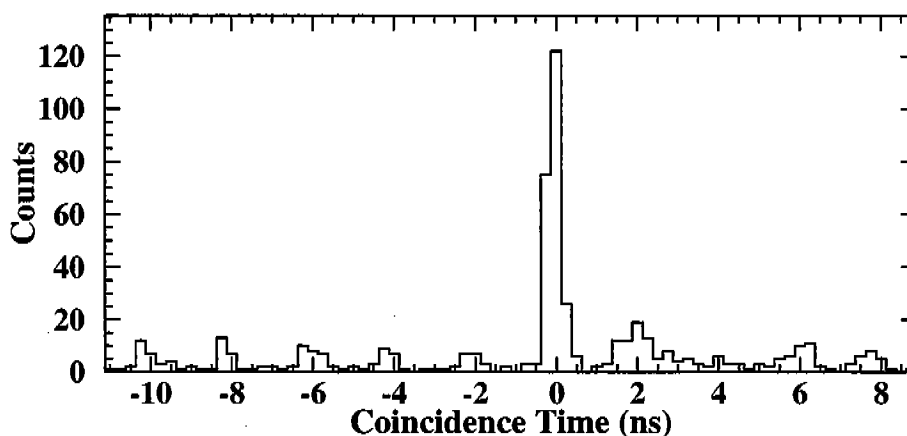


FIG. 7. Coincidence time spectrum between the electron and the hadron arms.

In this particular plot, the coincidence time window ( $\sim 30$  ns of which  $\sim 20$  ns is shown) allows identification of not only the true coincident kaons but also the kaons coming from random coincidences. The latter are subtracted from the real coincident kaons in the offline analysis. The 2 ns structure of the CEBAF beam is also clearly visible.

#### E. $\Sigma^0$ identification

From the sample of kaons identified as explained in the previous section, the missing mass of the undetected particles can be reconstructed (Fig. 8).

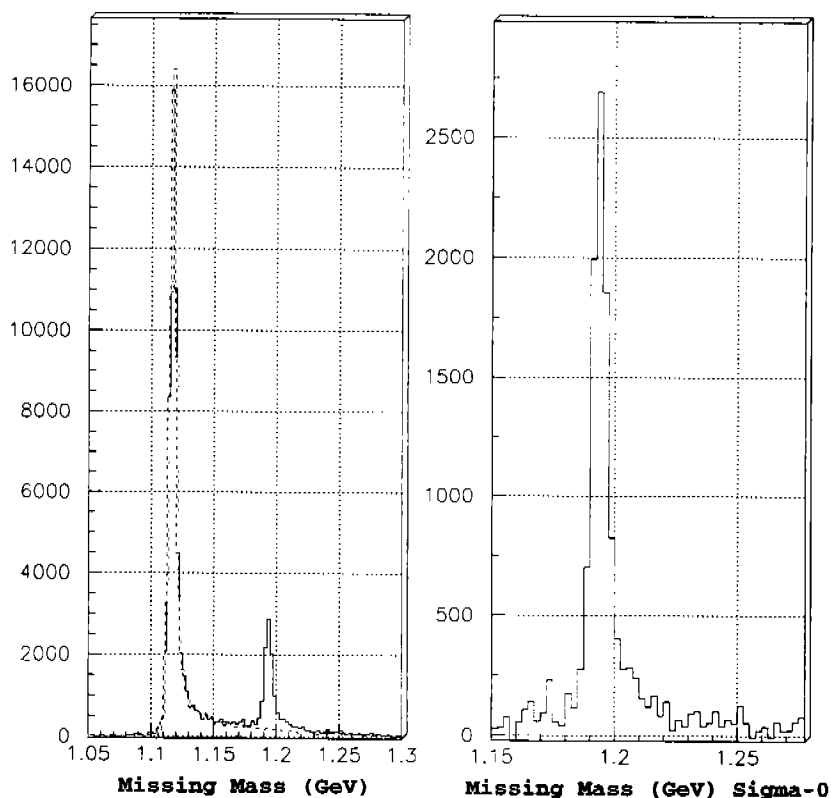


FIG. 8. Left: typical missing mass spectrum for electron-kaon coincidence events. The dashed line correspond to the Monte Carlo [59] which will be used to subtract the tail underneath the  $\Sigma^0$  peak. Right: the  $\Sigma^0$  missing mass after subtraction of the  $\Lambda$  radiative tail.

Clear peaks at the  $\Lambda$  and  $\Sigma^0$  masses are reconstructed. From this spectrum, the separation of  $\Sigma^0$  events can be performed easily [9]. The experiment described in this proposal will use the same techniques to identify the  $\Sigma^0$  hyperon from the  $\gamma_\nu + p \rightarrow K + Y(\Lambda, \Sigma^0)$  reaction.

#### 1. Hydrogen target and incident electron beam

The proposed experiment will use the Hall C standard 4 cm unpolarized liquid hydrogen target. This target container is cylindrical in shape and has 0.1 mm thick aluminum end-windows. The uncertainty in the target length and target density is expected to be about 0.5%. For the density, the calculated value based upon 19.0 K temperature and 16 psi pressure (operating parameters) is  $0.070 \text{ g/cm}^3$ . For each point, a dummy target and target full run will be taken in order to determine the background contribution coming from the target walls.

This experiment will use the unpolarized 1.5 GHz electron beam from the CEBA machine at Jefferson Lab with a current of about  $30 \mu\text{A}$  or more. The beam current will be measured using the standard Hall C beam current monitors.

## 2. Electronics and trigger

The proposed experiment will use the CEBAF Online Data Acquisition (CODA) system developed at Jefferson Lab. The trigger in the HMS detector will consist of  $S_3.C_G$  for three out-of-four (3/4) scintillators ( $S_3$ ), and the gas Čerenkov  $C_G$  detector signals to separate out electrons from pions, kaons and antiprotons. The SOS will use the  $S_3.C_A$  for 3/4 scintillators ( $S_3$ ), the gas Čerenkov  $C_G$  and the aerogel Čerenkov  $C_A$  (as a veto) detector signals to separate out kaons from pions (and positrons).

## 3. Expected systematic uncertainties

We will make use of the previous kaon experiments [56,57] to estimate the uncertainties associated with each detector element. They are summarized in Table V.

|                                     |           |
|-------------------------------------|-----------|
| Counter dead time                   | 1.5%      |
| Wire chamber inefficiencies         | 0.5%      |
| HMS shower counter inefficiencies   | 1.0%      |
| SOS Čerenkov counter inefficiencies | 2.0%      |
| Kaon absorption (target/detectors)  | 1.0%      |
| Kaon decay                          | 3.0%      |
| Knock-on events firing SOS Čerenkov | 1.0%      |
| Target wall events                  | 0.5%      |
| Randoms                             | 1.0%      |
| In time kaon losses                 | 1.0%      |
| Radiative corrections               | 3.0%      |
| Acceptance correction               | 2.0%      |
| <b>Total</b>                        | <b>6%</b> |

TABLE V. Expected systematic corrections.

A 6% total systematic uncertainty is expected due to the various corrections listed above.

### F. Monte Carlo Simulation

Our Monte Carlo simulation is described in detail in [59]. The main goals of this simulation were to evaluate the expected invariant mass distribution for the  $\Delta^*$  resonances and the exotic states. In what follows, we will focus on the  $e + p \rightarrow e' + K^+ + \Sigma^0$  reaction. The procedure is analogous for the  $e + p \rightarrow e' + p' + \pi^0$  reaction.

Considering the reaction  $e + p \rightarrow e' + K^+ + \Sigma^0$ , 6 quantities are necessary to characterize completely the reaction in the laboratory system (Fig. 9):

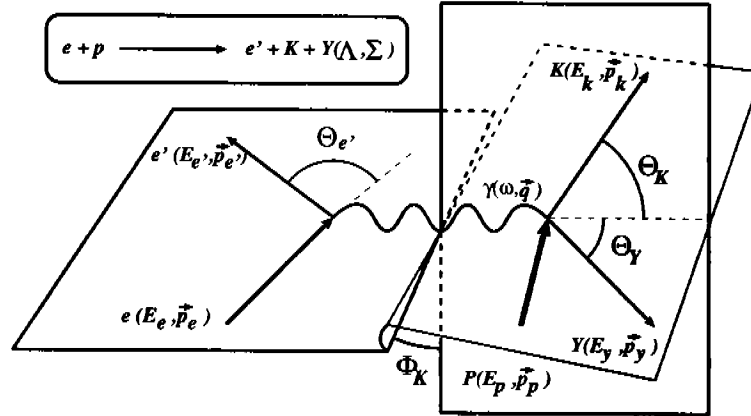


FIG. 9. The leptonic and hadronic plans for the reaction  $p(e, e'K)Y(\Lambda, \Sigma^0)$ .

- Incident electron: the energy ( $E_e$ ) is randomly generated within a  $10^{-3}$  resolution to match the actual Hall C energy accuracy.
- Scattered electron: the momentum and angles ( $P_{e'}$ ,  $\theta_{e'}$ ,  $\phi_{e'}$ ) are generated uniformly within the HMS angular and momentum acceptances.
- Electro-produced kaon: the direction ( $\theta_K$ ,  $\phi_K$ ) of the momentum  $\vec{P}_K$  is generated uniformly within the SOS angular acceptance.

From these quantities and using the conservation of energy and momentum, one can evaluate the energy  $E_\Sigma$  and the momentum  $\vec{P}_\Sigma$  of the  $\Sigma$ -hyperon.

In addition, the position ( $X_{\text{tar}}$ ,  $Y_{\text{tar}}$ ,  $Z_{\text{tar}}$ ) of each event is also randomly generated at the target. In order to make this Monte Carlo as close as possible to reality, we have used the standard operating conditions of Hall C: 4.36 cm liquid hydrogen target characteristics, typical  $100 \times 50 \mu\text{m}$  ellipsoid beam spot size of the CEBA machine, as well as different raster sizes (to test the influence of the beam spot size on the reconstructed distributions).

From the momentum ( $P_{\text{tar}}$ ), position ( $X_{\text{tar}}$ ,  $Y_{\text{tar}}$ ) and angles ( $X'_{\text{tar}}$ ,  $Y'_{\text{tar}}$ ) of the particle at the target (entrance of each spectrometer), the code transports the particle inside the detector hut using the COSY [60] forward matrix elements to give the corresponding parameters at the focal plane. The COSY backward matrix elements are then used to transport the particle back to the target and give the reconstructed parameters. Using the conservation of the momentum and the energy, the missing particle quantities (energy, momentum, and mass) are computed.

These calculations include the energy loss and multiple scattering correction of the particle while travelling through all materials from the target to the last element inside the detector hut as well as radiative corrections which were applied to all charged particles involved in the reaction.

Each resulting spectrum is then weighted by the appropriate correction factors: radiative corrections, decay probability (of the kaon), theoretical cross section (see appendix A), ...

The simulation was run for all kinematic settings listed in Table III. We show in Fig. 10 the expected invariant mass distribution obtained for the  $\Sigma^0$  from the  $p(e, e'K^+)\Sigma^0$  reaction at  $Q^2 = 0.75 \text{ (GeV/c)}^2$ .

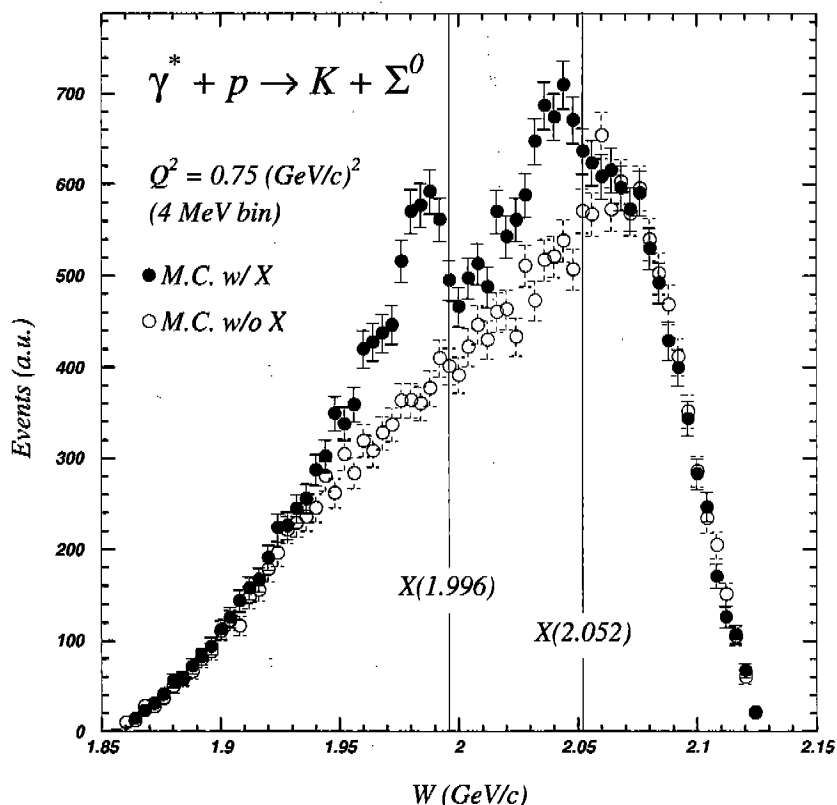


FIG. 10. Expected invariant mass distribution of the  $\Sigma^0$  at  $Q^2 = 0.75 \text{ (GeV/c)}^2$  without (empty circles) and with (solid circles) the X resonances. The solid [dashed] line shows the location of the X(1999) [X(2052)].

The inclusion of the X-resonances induces an increase of the cross section in the region between 1.9 and 2 GeV in the vicinity of the expected X(1999), and between 2.03 and 2.06 GeV in the vicinity of the expected X(2052). The acceptance coverage in  $W$  is sufficient to clearly show the two prominent enhancements. We would like to stress that our Monte Carlo simulation does not include any  $Q^2$  dependence of these resonances.

#### G. Preliminary results of an experimental test

On December 13, 1999, an experimental test was performed during the second stage of experiment E91016 [57]. Data were collected during a total time of 2 hours at the invariant mass of 1.925 GeV.

The kinematic setting, beam characteristics and reconstructed quantities are listed in Table VI.

| Item                     | Comments                        |
|--------------------------|---------------------------------|
| Reaction                 | $p(e, e' K)[\Lambda, \Sigma^0]$ |
| $I_{\text{beam}}$        | 30 $\mu\text{A}$                |
| $E_{\text{beam}}$        | 3.245 GeV                       |
| $P_{\text{HMS}}$         | 1.432 GeV/c                     |
| $\theta_{\text{HMS}}$    | 19.64°                          |
| $P_{\text{SOS}}$         | 1.290 GeV/c                     |
| $\theta_{\text{SOS}}$    | 14.23°                          |
| $W$                      | 1.925 GeV                       |
| $Q^2$                    | 0.55 (GeV/c) <sup>2</sup>       |
| Total coincidence events | 122596                          |
| Dummy events             | 17454                           |
| Corrected missing mass   | 11910                           |

TABLE VI. Experimental conditions for the test run performed on December 13, 1999.

The results of the analysis are displayed in Figs. 11 and 12, and 13.

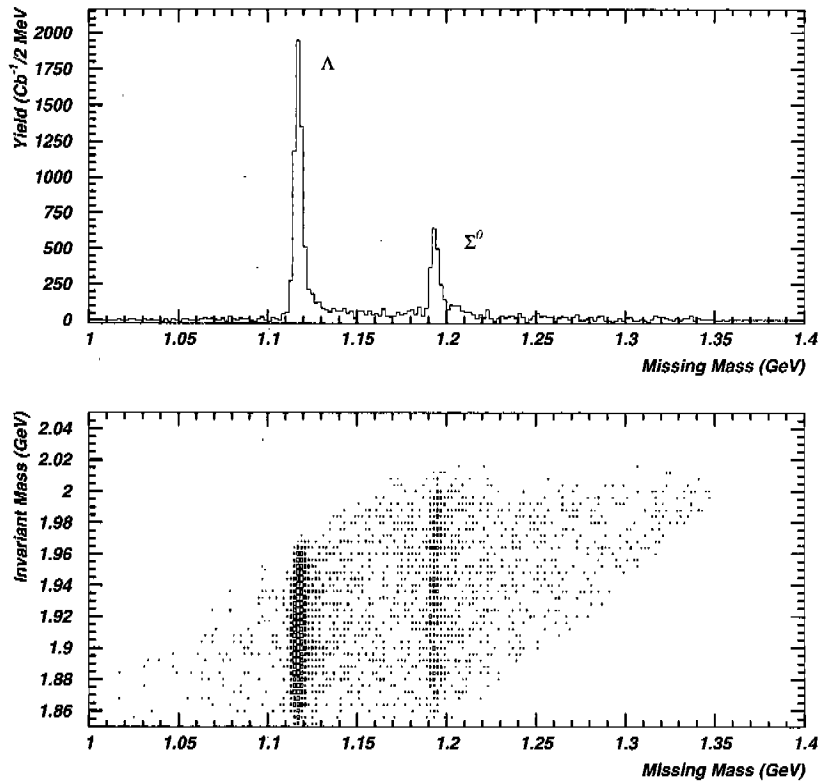


FIG. 11. Missing mass and invariant mass distributions obtained during the test run on December 13, 1999. Top: Missing mass distribution. Bottom: Invariant mass versus missing mass.

**Fig. 11:** The top panel shows the charge normalized number of events corrected from accidentals and contamination from the cell walls of the beer can as a function of the missing mass. The two hyperons produced during the reaction can be seen at their expected location:  $\Lambda$ (1.116 GeV) and  $\Sigma^0$ (1.189 GeV). The bottom panel shows the invariant mass ( $W$ ) as a function of the missing mass. The test run was kinematically set to put the  $\Sigma^0$  in the middle of the acceptance in  $W$ .

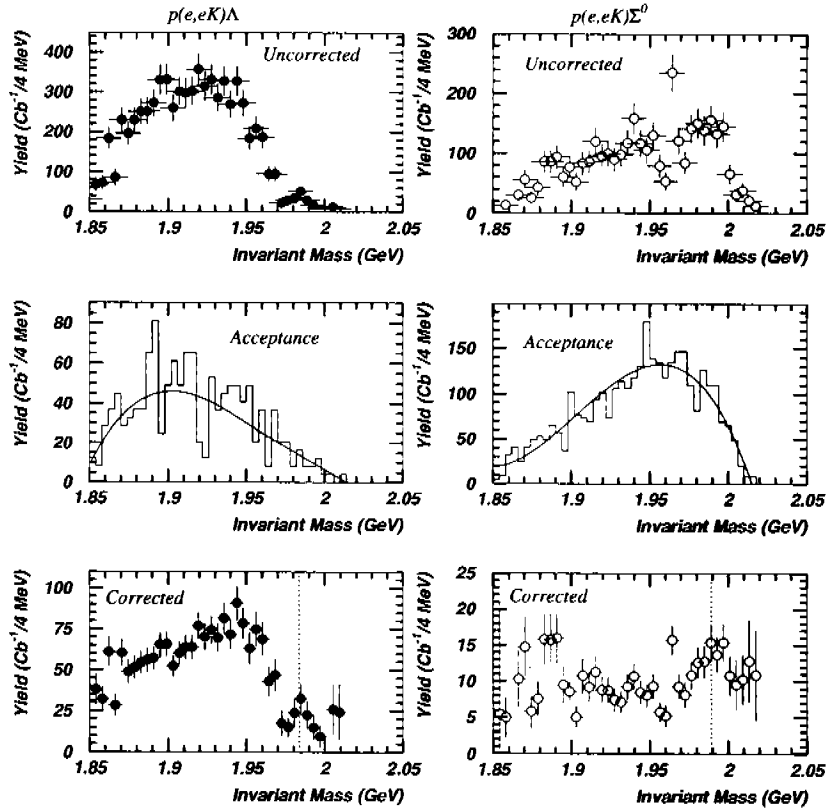


FIG. 12. Invariant mass distributions obtained during the test run on December 13, 1999 for the  $\Lambda$  (left column) and  $\Sigma^0$  (right column). Top: Reconstructed invariant mass. Middle: Acceptance of the apparatus used to performed the experiment. Bottom: Acceptance corrected invariant mass distributions.

**Fig. 12:** The invariant mass distributions for the  $\Lambda$  (left column) and the  $\Sigma^0$  (right column). The top panel shows the number of events as a function of  $W$  reconstructed for each hyperon. The middle panel shows the acceptance of the experimental setup for both  $W$  distributions. The bottom panel corresponds to the ratio between the top panel and the middle panel (acceptance corrected yield). The result of gaussian fits of the enhancements at 1.966 GeV (in the  $\Sigma^0$  channel only and 1.986 GeV (in both  $\Lambda$  and  $\Sigma^0$  channels) are listed in Table VII.

| Item                        | Comments                    |
|-----------------------------|-----------------------------|
| Counts in $W(\Sigma^0)$     | 822 (6.9% of overall)       |
| Counts in $W = 1.989$ GeV   | 200 (24.33% of $\Sigma^0$ ) |
| $M_{\Sigma^0}^1(X)$         | $(1989.2 \pm 7.9)$ MeV      |
| $\sigma_{\Sigma^0}^1(X)$    | $(16.097 \pm 14.951)$ MeV   |
| $ \chi^2/Ndf _{\Sigma^0}^1$ | 0.026/8                     |
| Counts in $W = 1.966$ GeV   | 53 (6.45% of $\Sigma^0$ )   |
| $M_{\Sigma^0}^2(X)$         | $(1966.1 \pm 6.9)$ MeV      |
| $\sigma_{\Sigma^0}^2(X)$    | $(4.006 \pm 6.006)$ MeV     |
| $ \chi^2/Ndf _{\Sigma^0}^2$ | 10.72/4                     |
| Counts in $W(\Lambda)$      | 1683 (14.13% of overall)    |
| Counts in $W = 1.983$ GeV   | 7 (0.4% of $\Lambda$ )      |
| $M_{\Lambda}(X)$            | $(1983.5 \pm 1.3)$ MeV      |
| $\sigma_{\Lambda}(X)$       | $(6.984 \pm 1.312)$ MeV     |

TABLE VII. Results from the test run performed on December 13, 1999.

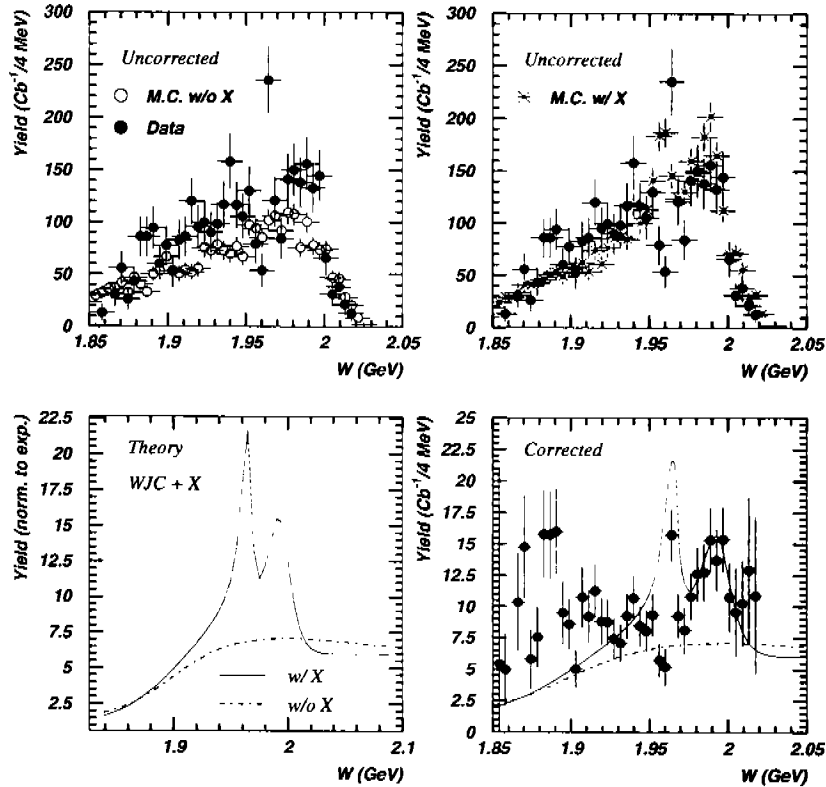


FIG. 13. Invariant mass distribution of the  $\Sigma^0$  obtained during the test run on December 13, 1999. Top: Data compared to a simulation of the experiment. Bottom: Data compared to a theoretical calculation.

**Fig. 13:** The invariant mass distribution of the  $\Sigma^0$  from the data is compared to a Monte Carlo simulation and a theoretical calculation. The top panel shows the data (solid points) compared to our best knowledge of the apparatus without (top-left: open points) and with (top-right: stars) including the possibility of existence of exotic systems. A better agreement with the experiment is observed in the top right panel when the assumption of exotic systems is made. The bottom panel shows a comparison of a theoretical prediction with the data. The bottom left panel is the prediction from a model that assumes (solid line) or not (dot-dashed line) the existence of the narrow resonances with Breit-Wigner shapes fitted to the one observed in the test. On the bottom right figure, the theory is compared to the data after acceptance correction. The model under-estimate the data for  $W < 1.9$  GeV as observed in the SAPHIR data when one does not take into account the possible  $D_{13}(1895)$  missing resonance [29] predicted by the relativistic quark model of Roberts and Capstick [32]. Our model used here, does not include this resonance. Also, a new resonance at 1.966 GeV seems to show up. This, if it is confirmed, will be a completely new experimental result.

The overall  $\Sigma^0$  production is about 822 counts. The datum at  $W = 1.966$  GeV corresponds to about 53 counts above the background. In other words, 6.9% of  $\Sigma^0$  is produced, and 6.5% (24%) of the  $\Sigma^0$  production falls in the expected missing resonance at 1.966 GeV (1.986 GeV). These results confirm our rate estimation, originally calculated using the electro-production data from E93018 [56] and photo-production data from SAPHIR. [30] (see section IV H below).

## H. Requested Beam Time

The estimated singles and coincident rates were calculated using:

$$R_{e,K(p)} = \left( \frac{d\sigma}{d\Omega_{e',K(p)}} \right)_{\text{Lab}} \cdot N_e \frac{Nt}{A} \Delta\Omega_{e',K(p)}, \quad (19)$$

$$R_{\text{coin}} = \left( \frac{d^3\sigma}{d\Omega_{e'} d\Omega_{K(p)} dE_{e'}} \right)_{\text{Lab}} \cdot N_e \frac{Nt}{A} \Delta\Omega_{e'} \Delta E_{e'} \Delta\Omega_{K(p)}, \quad (20)$$

where  $\left( \frac{d\sigma}{d\Omega_{e',K(p)}} \right)_{\text{Lab}}$  and  $\left( \frac{d^3\sigma}{d\Omega_{e'} d\Omega_{K(p)} dE_{e'}} \right)_{\text{Lab}}$  are the single and coincident cross sections in the laboratory. Since the pion production is higher than the kaon production in our kinematic settings, we will consider only the kaon cross section for the rate estimation. The cross section for kaon production was estimated from the kaon experiments [8,9].  $N_e$  is the number of incident electrons (for a 30  $\mu\text{A}$  beam) within 1 sec,  $\frac{Nt}{A}$  the number of target nuclei (for a 4.36 cm liquid hydrogen target),  $\Delta\Omega_{e'}$  ( $\Delta\Omega_K$ ) is the HMS (SOS) solid angle and  $\Delta E_{e'}$  the scattered electron energy binning taken to be 1 MeV. For  $X$  rates, we have used the photo-production data from SAPHIR [30] and extrapolated to electro-production assuming a  $Q^{-8}$  fall-off.

During the previous kaon experiments, the singles rates for a 35  $\mu\text{A}$  beam current and a 4 cm liquid hydrogen target were in average found to be around 10 kHz in the electron arm (well below the design limit of the HMS detectors) and 1 MHz in the (SOS) hadron arm which is adequate for this proposed experiment.

The estimate of the accidental to true (A/T) coincidences was obtained from:

$$\frac{A}{T} = \frac{\tau \times R_e \times R_K}{R_{\text{coinc}} \times d.f.} \quad (21)$$

$R_{e(K)}$  is the single rate for electron (kaon) production measured in the HMS (SOS),  $\tau$  is the resolving time taken to be 1 ns offline and 30 ns online, and  $d.f.$  is the 100% duty factor of the CEBA machine. During the previous kaon experiments [56,57], an offline ratio  $A/T$  of 1/100 was achieved.

For 10,000  $\Sigma^0$  at each  $Q^2$  setting, between 100-2,000  $X$  events will be extracted, depending on the kinematics. A **total beam time of 15 days** is requested to cover the kinematic settings listed in Table III which will measure the  $W$  distributions of the region of interest at fifteen (15) different  $Q^2$ : 11 days will be dedicated for real data taking and an additional 4 days for various calibrations, spectrometer settings, ...

| $Q^2$<br>(GeV/c) <sup>2</sup> | $W$<br>(GeV/c) | $\left( \frac{d\sigma}{d\Omega_K d\Omega_{e'} dE_{e'}} \right)_{\text{Lab}}$<br>(nb/sr) | $\Sigma^0$ -Rate<br>(sec <sup>-1</sup> ) | $X$ -Rate<br>(% of $\Sigma^0$ ) | Days |
|-------------------------------|----------------|---|--|---------------------------------|------|
| 0.52                          | 1.840          | 390   | 0.67                                     | -                               | 0.19 |
| 0.75                          | 1.840          | 298   | 0.51                                     | -                               | 0.25 |
| 1.00                          | 1.810          | 157   | 0.28                                     | -                               | 0.47 |
| 0.55                          | 1.901          | 697   | 0.16                                     | -                               | 0.80 |
| 0.65                          | 1.900          | 627   | 0.14                                     | -                               | 0.91 |
| 0.75                          | 1.900          | 552   | 0.12                                     | -                               | 1.06 |
| 0.85                          | 1.900          | 474   | 0.10                                     | -                               | 1.27 |
| 0.95                          | 1.901          | 399   | 0.08                                     | -                               | 1.59 |
| 1.05                          | 1.901          | 211   | 0.04                                     | -                               | 3.18 |

|              |       |     |      |     |              |
|--------------|-------|-----|------|-----|--------------|
| 0.45         | 2.001 | 734 | 1.26 | 18  | 0.10         |
| 0.55         | 2.001 | 706 | 1.21 | 8   | 0.10         |
| 0.65         | 2.000 | 687 | 1.18 | 4   | 0.11         |
| 0.75         | 2.000 | 674 | 1.16 | 2   | 0.11         |
| 0.85         | 2.000 | 664 | 1.14 | 1   | 0.11         |
| 0.95         | 2.000 | 656 | 1.13 | 0.6 | 0.11         |
| 1.05         | 2.001 | 648 | 1.11 | 0.4 | 0.11         |
| <b>Total</b> |       |     |      |     | <b>10.47</b> |

TABLE VIII. The estimated rates and beam time.

## V. MISCELLANEOUS

In Table VIII, one would notice that an increase in the beam energy will favor higher counting rates. For example, a beam energy of about 5 GeV, gives a  $\Sigma^0$  production rate 5-10% higher than at 4 GeV. However, the kinematics will be constrained by the physical angular range of the SOS spectrometer.

Another important point is the fact that the experiment described in this document is based on a correlated kinematic settings, i.e., coincidence experiment. The fact that the invariant mass range is already fixed (about 2 GeV) and that, in the case of the  $X$ , the production rate is very small (a few percent of  $\Sigma^0$  events), favor a high luminosity experiment. For example, running the same experiment in Hall B at Jefferson Lab (where typical beam current for electron running is on the order of a few nA compare to about 50  $\mu$ A in Hall C) would require years of running time to acquire the equivalent number of events in both  $\Delta^*$  and  $X$ . In addition, multi-pion production are favored in the invariant mass range proposed in this experiment which induces a large background for a  $4\pi$  detector like CLAS in Hall B, while easy missing mass technique can be used in Hall C for the  $\Delta^*$  resonances. In the case of the  $X$ , small binning and true differential cross section are needed to obtain reliable information with the technique used in this document. This is another weak point for a  $4\pi$  detector where all the  $\Sigma^0$  produced will be distributed in a wide range and the resolution of CLAS implies a much bigger energy bin than the one in Hall C (typical 20 MeV compares to 2 MeV) which can certainly washed out any narrow resonance with small cross section production. However, the data provided will be complementary of angular distributions that can be obtained from Hall B.

## VI. CONCLUSION

In this document, we propose the study of the excited intermediate states associated with electro-production of  $K^+$  mesons. The  $Q^2$  dependence of three excited nucleon resonances,  $\Delta^*(1900)$ ,  $\Delta^*(1910)$ , and  $\Delta^*(1920)$ , will be performed as well as a study of the crypto-exotic baryon X(2000). Data from this experiment will be unprecedented with such level of precision at non-zero four-momentum transfer. Information on SU(3) violation in the strangeness channel will be extracted, sensitivity to transition form factors in kaon electro-production will be obtained, new additional constraints on Regge-type models in the intermediate energy regime could be evaluated, and the experimental evidence of missing resonances and/or exotic systems could be proven. A beam time of 15 days is requested to cover the necessary invariant mass region for four-momentum transfer ranging from 0.55 to 1.05 (GeV/c)<sup>2</sup>.

## APPENDIX A: FORMALISM OF THE (E,E'K)Y REACTION

To establish the notation for explicit discussion, let us consider the electro-production reaction:

$$e(e_1) + p(p) \rightarrow e'(e_2) + K^+(k) + Y(l), \quad (\text{A1})$$

where each particle's 4-momentum is labeled in parentheses. The virtual photon momentum is defined to be  $q = e_1 - e_2$ . The Feynman diagrams correspond to those on Fig. 5. In the one-photon exchange approximation, the transition amplitude for hyperon  $Y = \Lambda, \Sigma$  production is expressed as the invariant product of leptonic ( $\mathcal{L}^\mu$ ) and hadronic ( $\mathcal{H}_Y^\mu$ ) currents mediated by the photon propagator,  $g_{\mu\nu}/q^2$ :

$$t_Y = \frac{\mathcal{L} \cdot \mathcal{H}_Y}{q^2}. \quad (\text{A2})$$

The unpolarized differential cross section is calculated from the spin averaged squared transition amplitude

$$\langle |t_Y|^2 \rangle = \frac{1}{4} \sum_{s_1, s_2} \sum_{\lambda, \lambda'} |e \bar{u}_{e'}(e_2, s_2) \frac{\gamma_\mu}{q^2} u_e(e_1, s_1) \mathcal{H}_Y^\mu(\lambda, \lambda')|^2 \quad (\text{A3})$$

$$= \frac{e^2}{4q^4 M_e^2} \sum_{\lambda, \lambda'} \left[ \frac{1}{2} q^2 |\mathcal{H}_Y(\lambda, \lambda')|^2 + 2 |e_1 \cdot \mathcal{H}_Y(\lambda, \lambda')|^2 \right], \quad (\text{A4})$$

where for each external spin 1/2 particle carrying 4-momentum  $x$  and spin projection  $\lambda$ , we associate a Dirac spinor  $u(x, \lambda)$ . The hadronic current is explicitly conserved through the decomposition:

$$\mathcal{H}_Y^\mu(\lambda, \lambda') = \bar{u}_Y(l, \lambda') \left[ \sum_{i=1}^6 B_i(s, t, q^2) \mathcal{N}_i^\mu \right] u_p(p, \lambda). \quad (\text{A5})$$

The  $B_i(s, t, q^2)$  factors are the so-called invariant (or covariant Feynman) amplitudes, which are scalar functions of the Lorentz invariant Mandelstam variables, and the  $\mathcal{N}_i^\mu$  terms form a complete basis of gauge invariant matrices (Dirac operators):

$$N_\mu^1 = \frac{1}{2} \gamma_5 (\gamma \cdot q \gamma_\mu - \gamma_\mu \gamma \cdot q), \quad (\text{A6})$$

$$N_\mu^2 = \gamma_5 \left( p_\mu - \frac{p \cdot q}{q^2} q_\mu \right), \quad (\text{A7})$$

$$N_\mu^3 = \gamma_5 \left( l_\mu - \frac{l \cdot q}{q^2} q_\mu \right), \quad (\text{A8})$$

$$N_\mu^4 = \gamma_5 (p \cdot q \gamma_\mu - \gamma \cdot q p_\mu), \quad (\text{A9})$$

$$N_\mu^5 = \gamma_5 (l \cdot q \gamma_\mu - \gamma \cdot q l_\mu), \quad (\text{A10})$$

$$N_\mu^6 = \gamma_5 (\gamma \cdot q q_\mu - q^2 \gamma_\mu). \quad (\text{A11})$$

Another useful decomposition of the hadronic current involves the definition of Chew, Goldberger, Low, and Nambu (CGLN) amplitudes  $\mathcal{F}_i$  [61]:

$$\vec{\mathcal{H}}(\lambda', \lambda) = \chi_{\lambda'}^T \left[ \sum_{i=1}^6 \vec{\mathcal{H}}_i \right] \chi_\lambda, \quad (\text{A12})$$

where

$$\vec{\mathcal{H}}_i = \left( \frac{4\pi\sqrt{s}}{\sqrt{M_p M_\Lambda}} \right) \mathcal{F}_i \vec{\mathcal{P}}_i. \quad (\text{A13})$$

The CGLN amplitudes are coefficients of Pauli spin operators,  $\vec{\mathcal{P}}_i$  defined as:

$$\vec{\mathcal{P}}_1 = (\vec{\sigma} - \vec{\sigma} \cdot \hat{q} \hat{q}) \quad (\text{A14})$$

$$\vec{\mathcal{P}}_2 = i\vec{\sigma} \cdot \hat{k} (\vec{\sigma} \times \hat{q}) \quad (\text{A15})$$

$$\vec{\mathcal{P}}_3 = (\hat{k} - \hat{k} \cdot \hat{q} \hat{q}) \vec{\sigma} \cdot \hat{q} \quad (\text{A16})$$

$$\vec{\mathcal{P}}_4 = (\hat{k} - \hat{k} \cdot \hat{q} \hat{q}) \vec{\sigma} \cdot \hat{k} \quad (\text{A17})$$

$$\vec{\mathcal{P}}_5 = \hat{q} (\vec{\sigma} \cdot \hat{q}) \quad (\text{A18})$$

$$\vec{\mathcal{P}}_6 = \hat{q} (\vec{\sigma} \cdot \hat{k}), \quad (\text{A19})$$

where  $\vec{\sigma}$  are the Pauli matrices and  $\hat{q}$  ( $\hat{k}$ ) is the photon (kaon) 3-momentum unit vector. Note that the first four terms correspond to the transverse hadronic current since  $\hat{q} \cdot \vec{\mathcal{H}}_i = 0$  for  $(i = 1, 2, 3, 4)$ , and the last two terms define the longitudinal hadronic current since there is a non-zero projection onto the photon momentum direction. The Pauli spin operators and CGLN amplitudes are derived from a non-relativistic reduction of the covariant current expression. In terms of the invariant amplitude functions (obtained from the covariant Feynman rules)  $B_i$ , the CGLN amplitudes are expressed:

$$\mathcal{F}_1 = N [ B_1 (|\vec{q}|Q + q_0) - B_4 q \cdot p - B_5 q \cdot l + B_6 q^2 ] \quad (\text{A20})$$

$$\mathcal{F}_2 = N [ -B_1 K (|\vec{q}| + q_0 Q) - B_4 q \cdot p Q K - B_5 q \cdot l Q K + B_6 q^2 Q K ] \quad (\text{A21})$$

$$\mathcal{F}_3 = N [ B_3 |\vec{k}| Q + B_5 |\vec{k}| (|\vec{q}| + q_0 Q) ] \quad (\text{A22})$$

$$\mathcal{F}_4 = N [ -B_3 |\vec{k}| K + B_5 |\vec{k}| K (|\vec{q}| Q + q_0) ] \quad (\text{A23})$$

$$\mathcal{F}_5 = N [ B_1 q_0 + B_2 |\vec{q}| Q (1 + \frac{q \cdot p}{q^2}) + B_3 Q (|\vec{q}| \frac{q \cdot l}{q^2} + |\vec{k}| \cos \theta) \quad (\text{A24})$$

$$+ B_4 q_0 (|\vec{q}| Q - p_0) + B_5 (|\vec{k}| \cos \theta (|\vec{q}| + q_0 Q) - q \cdot l) + B_6 q_0 (q_0 + |\vec{q}| Q) ]$$

$$\mathcal{F}_6 = N [ -B_1 q_0 Q K - B_2 |\vec{q}| K (1 + \frac{q \cdot p}{q^2}) - B_3 K (|\vec{q}| \frac{q \cdot l}{q^2} + |\vec{k}| \cos \theta) \quad (\text{A25})$$

$$+ B_4 q_0 K (|\vec{q}| - p_0 Q) + B_5 (|\vec{k}| K \cos \theta (|\vec{q}| Q + q_0) - K Q q \cdot l)$$

$$+ B_6 |\vec{q}| K (q_0 + |\vec{q}| Q) + q^2 Q K ],$$

where  $N$  is a normalization factor

$$N = \frac{\sqrt{(l_0 + M_\Lambda)(p_0 + M_p)}}{8\pi\sqrt{s}}, \quad (\text{A26})$$

and  $Q, K$  are dimensionless functions:

$$K = \frac{|\vec{k}|}{l_0 + M_\Lambda} \quad Q = \frac{|\vec{q}|}{p_0 + M_p}. \quad (\text{A27})$$

All energy and momentum factors are evaluated in the center of mass system.

Let us consider the observables where the spin of the produced hyperon is detected. The polarization of the final-state hyperon is defined as the asymmetry in the differential cross section between spin-up and spin-down hyperon production. One technique to calculate the polarized cross section

is to employ a covariant spin projection operator to determine the spin-up and spin-down hadronic current [62],

$$\Pi(\uparrow\downarrow) = \frac{1}{2}(1 \pm \gamma_5 \gamma \cdot \xi). \quad (\text{A28})$$

$\xi_\mu$  is a space-like unit-4 vector which defines the spin quantization axis. The polarized hadronic current is:

$$\mathcal{H}_Y^\mu(\uparrow\downarrow) = \bar{u}_Y(l, \lambda') \bar{\Pi}(\uparrow\downarrow) \left[ \sum_{i=1}^6 B_i(s, t, q^2) \mathcal{N}_i^\mu \right] u_p(p, \lambda). \quad (\text{A29})$$

Another standard technique is to use a spin density matrix formalism to calculate polarization observables in terms of the Pauli spin operators of the CGLN current decomposition [63,64]. As an example, the longitudinal cross section can be defined as the squared  $z$ -component of the hadronic current:

$$\mathcal{H}_z = \hat{q}(\vec{\sigma} \cdot \hat{q}) \mathcal{F}_5 + \hat{q}(\vec{\sigma} \cdot \hat{k}) \mathcal{F}_6, \quad (\text{A30})$$

$$\sigma_L \equiv \frac{d\sigma_L}{d\Omega_K} = \frac{|\vec{k}|}{|\vec{q}|} \sum_\lambda \chi_\lambda^T |\mathcal{H}_z|^2 \chi_\lambda, \quad (\text{A31})$$

$$\begin{aligned} &= \frac{|\vec{k}|}{|\vec{q}|} \sum_\lambda \chi_\lambda^T \left[ (\vec{\sigma} \cdot \hat{q})^2 |\mathcal{F}_5|^2 + (\vec{\sigma} \cdot \hat{k})^2 |\mathcal{F}_6|^2 + \right. \\ &\quad \left. 2(\vec{\sigma} \cdot \hat{q})(\vec{\sigma} \cdot \hat{k}) \Re[\mathcal{F}_5 \mathcal{F}_6^*] \right] \chi_\lambda. \end{aligned} \quad (\text{A32})$$

Using the identities:

$$(\vec{\sigma} \cdot \hat{a})(\vec{\sigma} \cdot \hat{b}) = \hat{a} \cdot \hat{b} + i\vec{\sigma} \cdot (\hat{a} \times \hat{b}), \quad (\text{A33})$$

$$\sum_\lambda \chi_\lambda^T [\vec{\sigma} \cdot (\hat{q} \times \hat{k})] \chi_\lambda = \sum_\lambda \chi_\lambda^T [\sin \theta \sigma_y] \chi_\lambda = 0, \quad (\text{A34})$$

$$\hat{q} \cdot \hat{k} = \cos \theta \quad (\text{A35})$$

we arrive at the expression for the longitudinal cross section in terms of the CGLN amplitudes:

$$\sigma_L = \frac{|\vec{k}|}{|\vec{q}|} \left[ \text{Re}\{|\mathcal{F}_5|^2 + |\mathcal{F}_6|^2 + 2 \cos \theta [\mathcal{F}_5^* \mathcal{F}_6]\} \right]. \quad (\text{A36})$$

The cross section for  $p(e, e'K)\Lambda$  can be written as follow:

$$\begin{aligned} \sigma &= \sigma_T + \epsilon_L \sigma_L + \sqrt{2\epsilon_L(1 + \epsilon_T)} \cos(\phi_{\gamma K}) \sigma_{TL} + \epsilon_T \cos(2\phi_{\gamma K}) \sigma_{TT} \\ &\quad + h\sqrt{2\epsilon_L(1 - \epsilon_T)} \sin(\phi_{\gamma K}) \sigma_{TL'} + h\sqrt{1 - \epsilon_T^2} \sigma_{TT'} \end{aligned} \quad (\text{A37})$$

In the same way then as  $\sigma_L$ , one can express  $\sigma_T$ ,  $\sigma_{LT}$ ,  $\sigma_{TT}$ ,  $\sigma_{TL'}$  and  $\sigma_{TT'}$  as a function of the CGLN amplitudes.

In fact, the general expression of the  $(\gamma_\nu, K)$  center of mass differential cross section is [65]:

$$\frac{d\sigma}{d\Omega_K^{\text{CM}}} = \frac{|\vec{k}|}{|\vec{q}|} P_\alpha P_\beta \left\{ R_T^{\beta\alpha} + \epsilon_L R_L^{\beta\alpha} \right\} \quad (\text{A38})$$

$$\begin{aligned}
& +\sqrt{2\epsilon_L(1+\epsilon_T)}[{}^cR_{TL}^{\beta\alpha}\cos(\phi_{\gamma_0K})+{}^sR_{TL}^{\beta\alpha}\sin(\phi_{\gamma_0K})] \\
& +\epsilon[{}^cR_{TT}^{\beta\alpha}\cos(2\phi_{\gamma_0K})+{}^sR_{TT}^{\beta\alpha}\sin(2\phi_{\gamma_0K})] \\
& +h\sqrt{2\epsilon_L(1-\epsilon_T)}[{}^cR_{TL'}^{\beta\alpha}\cos\phi_{\gamma_0K}+{}^sR_{TL'}^{\beta\alpha}\sin(\phi_{\gamma_0K})] \\
& +h\sqrt{1-\epsilon_T^2}R_{TT'}^{\beta\alpha}\}.
\end{aligned}$$

$P_\alpha = (1, \vec{\mathbf{P}})$  and  $P_\beta = (1, \vec{\mathbf{P}}')$  define the target and recoil polarized four vectors with  $\vec{\mathbf{P}} = (\mathbf{P}_x, \mathbf{P}_y, \mathbf{P}_z)$  and  $\vec{\mathbf{P}}' = (\mathbf{P}_{x'}, \mathbf{P}_{y'}, \mathbf{P}_{z'})$  the polarized three vector components, while  $h$  represents the helicity of the polarized incident electron beam. For an experiment with unpolarized beam, an unpolarized target and which does not measure the polarization of the emitted hyperon, this cross section reduces to:

$$\frac{d\sigma}{d\Omega_{\vec{K}}^{\text{CM}}} = \frac{|\vec{k}|}{|\vec{q}|} P_\alpha P_\beta \{ R_T^{00} + \epsilon_L R_L^{00} + \sqrt{2\epsilon_L(1+\epsilon_T)} {}^cR_{TL}^{00}\cos(\phi_{\gamma_0K}) + \epsilon {}^cR_{TT}^{00}\cos(2\phi_{\gamma_0K}) \}. \quad (\text{A39})$$

The  $R_i^{00}$  are function of six helicity amplitudes:

$$R_T^{00} = \frac{1}{2}(|H_1|^2 + |H_2|^2 + |H_3|^2 + |H_4|^2), \quad (\text{A40})$$

$$R_L^{00} = |H_5|^2 + |H_6|^2, \quad (\text{A41})$$

$${}^cR_{TL}^{00} = \frac{1}{\sqrt{2}}\text{Re}(H_5^*H_1 - H_5^*H_4 + H_6^*H_2 + H_6^*H_3), \quad (\text{A42})$$

$${}^cR_{TT}^{00} = \text{Re}(H_2^*H_3 - H_1^*H_4). \quad (\text{A43})$$

The transverse amplitudes ( $H_1, H_2, H_3, H_4$ ) can be measured via photo-production experiments while the longitudinal amplitudes ( $H_5, H_6$ ) require electro-production experiments.

These helicity amplitudes can be related to the six CGLN amplitudes [65] and define the spherical components ( $J_\pm = \pm(J_x \pm iJ_y)/\sqrt{2}$  and  $J_0 = J_z$ ) of the hadronic current operator  $\mathbf{J}$ :

$$J_+ = \begin{pmatrix} H_1 & H_2 \\ H_3 & H_4 \end{pmatrix}, \quad J_- = \begin{pmatrix} H_4 & -H_3 \\ -H_2 & H_1 \end{pmatrix}, \quad J_0 = \begin{pmatrix} H_5 & H_6 \\ H_6 & -H_5 \end{pmatrix}. \quad (\text{A44})$$

Determination of the six independent complex amplitudes (which uniquely describe the electro-production process) implies six absolute values and five relative phases between the CGLN amplitudes, i.e., eleven independent quantities to completely and uniquely determine the transition current  $\mathbf{J}$ .

Electro-production data are usually analyzed in terms of multipoles  $E_{l\pm}$ ,  $M_{l\pm}$ , and  $L_{l\pm}$  characterizing the excitation mechanism (electric  $E$ , magnetic  $M$  or longitudinal  $L$ ), the orbital  $l$  and total angular momentum  $j = l \pm \frac{1}{2}$ . The electromagnetic multipole radiations  $EL, ML, CL$  are responsible for resonance excitations ( $C$  stands for Coulomb). Their connection with the CGLN amplitudes can be established via multipole series in terms of derivatives of the Legendre polynomials  $P_l$  [66].

APPENDIX B:  $\Delta^* \rightarrow \pi N$  AND  $\Delta^* \rightarrow K\Sigma^0$  DECAY WIDTHS IN SU(3)

The expression of the decay width for a resonance  $R$  ( $J_R^{P_R}$ ) into a baryon  $B$  ( $J_B^{P_B}$ ) and a meson  $M$  ( $J_M^{P_M}$ ) can be written in the case of resonances with a spin  $s_R = 1/2, 3/2$  and  $5/2$  as

$$\Gamma_{\frac{1}{2}^\pm \rightarrow \frac{1}{2}^+ + 0^-} = \frac{g_{MBR}^2}{8\pi} \frac{[(M_R \mp M_B)^2 - M_M^2]}{M_R^2} |\mathbf{P}_M| \quad (\text{B1})$$

$$\Gamma_{\frac{3}{2}^\pm \rightarrow \frac{1}{2}^+ + 0^-} = \frac{g_{MBR}^2}{24\pi} \frac{[(M_R \pm M_B)^2 - M_M^2]}{M_R^2} |\mathbf{P}_M|^3 \quad (\text{B2})$$

$$\Gamma_{\frac{5}{2}^\pm \rightarrow \frac{1}{2}^+ + 0^-} = \frac{g_{MBR}^2}{60\pi} \frac{[(M_R \mp M_B)^2 - M_M^2]}{M_R^2} |\mathbf{P}_M|^5 \quad (\text{B3})$$

with, in our case, the meson  $M$  being a kaon or pion; the baryon  $B$  a proton,  $\Lambda$  or  $\Sigma$ ; and  $R$  the baryonic resonance.

The momentum of the meson (or baryon) in the resonance center-of-mass system is<sup>5</sup>

$$|\mathbf{P}_M|^2 = \frac{[(M_R - M_B)^2 - M_M^2][(M_R + M_B)^2 - M_M^2]}{4M_R^2}. \quad (\text{B4})$$

Therefore, the ratio of the decay widths for  $\Delta^* \rightarrow K^+\Sigma^0$  and  $\Delta^* \rightarrow \pi N$  can be expressed as

$$\frac{\Gamma_{\Delta^* \rightarrow K^+\Sigma^0}}{\Gamma_{\Delta^* \rightarrow \pi N}} = \left( \frac{g_{K\Sigma^0\Delta^*}}{g_{\pi N\Delta^*}} \right)^2 \left[ \frac{|\mathbf{P}_K|}{|\mathbf{P}_\pi|} \right]^{2l+1}. \quad (\text{B5})$$

In order to estimate this ratio, one needs both the center-of-mass momenta,  $\mathbf{P}_K$  and  $\mathbf{P}_\pi$ , and the strong coupling constants,  $g_{K\Sigma^0\Delta^*}$  and  $g_{\pi N\Delta^*}$ . However, the expression of the decay width ratio from relation (B5) is not completely correct since the general expression of the decay width depends on to which n-tuplet the resonance belongs to:

---

(a)  $R$  belongs to a singlet or decuplet  
(b)  $R$  belongs to an octet

$$\Gamma_{R \rightarrow B+M} = g_{MBR} \cdot c^2 \cdot \tau_{\text{kin}}^2$$

$$\Gamma_{R \rightarrow B+M} = [c_S \cdot g_S + c_A \cdot g_A]^2 \tau_{\text{kin}}'$$


---

<sup>5</sup>The exponents 1, 3 and 5 in Eq. (B1)-(B3) come from the  $2l+1$  power due to the spin contribution from the relative angular momentum  $l$  between the two clusters,  $M$  and  $B$ , in the resonance  $R$  having a parity  $P = (-1)^{l+1}$ .

where:  $g_{MBR}, g_S, g_A$  are the strong coupling constants;  $c, c_S, c_A$  the Clebsch-Gordan coefficients; and  $\tau_{\text{kin}}, \tau'_{\text{kin}}$  two kinematic factors.  $g_S$  ( $g_A$ ) is the strong coupling constant corresponding to the symmetric (anti-symmetric) octet<sup>6</sup>.

The three resonances of interest,  $\Delta(1900)[J^P = \frac{1}{2}^-, l = 0]$ ,  $\Delta(1910)[J^P = \frac{1}{2}^+, l = 1]$  and  $\Delta(1920)[J^P = \frac{3}{2}^+, l = 1]$ , belong to the three decuplets:  $\frac{1}{2}^-, \frac{1}{2}^+$ , and  $\frac{3}{2}^+$  in the SU(3) multiplet representation. Therefore, their decay widths obey the relation (a).

The Clebsch-Gordan coefficients can be obtained from the SU(3) amplitudes of the  $\Delta^*$  decays. The interaction Lagrangian computed from SU(3) for a decuplet as shown in Fig. 14 decaying into a baryon and a meson from the octets of Fig. 15 can be written as:

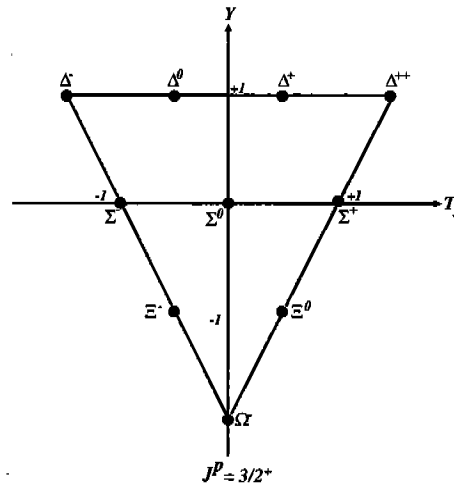


FIG. 14. The SU(3) baryon  $J^P = \frac{3}{2}^+$  decuplet in the  $(Y, T_3)$  representation.  $Y$  is the hypercharge and  $T_3$  the third component of the isospin.

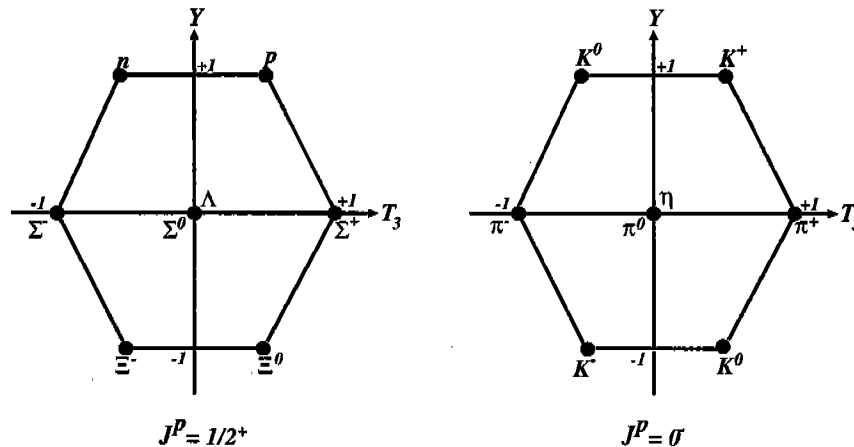


FIG. 15. The SU(3)  $J^P = \frac{1}{2}^+$  baryon and  $J^P = 0^-$  pseudo-scalar meson octets in the  $(Y, T_3)$  representation.

<sup>6</sup>In this case, since  $B$  and  $M$  belong to SU(3) octets,  $R$  belongs to the product:  $8 \otimes 8 = 27 \oplus 10 \oplus 10 \oplus 8_A \oplus 8_S \oplus 1$ . We find again here the singlet and decuplet with  $R$  having two components (two octets): one symmetric and one anti-symmetric.

$$\mathcal{L}_{\text{int}}^{10 \rightarrow 8 \oplus 8} = \sum \epsilon_{klm} T_{10}^{ijk} \bar{B}_8^{il} \Pi_8^{jm}, \quad (\text{B6})$$

where:  $T_{10}^{ijk}$  are the decuplet states (Table IX),  $B_8$  and  $\Pi_8$  are the octet states for the decay baryons and mesons, matrices (B7) and (B8), respectively. The  $i, j, k$  indices run from 1 to 3 and are SU(3) indices.

| $T_{10}^{ijk}$ | Baryon                        | $T_{10}^{ijk}$ | Baryon         | $T_{10}^{ijk}$ | Baryon         |
|----------------|-------------------------------|----------------|----------------|----------------|----------------|
| $T_{10}^{333}$ | $\Omega^-$                    | $T_{10}^{133}$ | $T_{10}^{313}$ | $T_{10}^{132}$ | $T_{10}^{312}$ |
| $T_{10}^{221}$ | $\frac{1}{\sqrt{3}} \Xi^0$    | $T_{10}^{313}$ | $T_{10}^{331}$ | $T_{10}^{312}$ | $T_{10}^{321}$ |
| $T_{10}^{211}$ | $\frac{1}{\sqrt{3}} \Xi^-$    | $T_{10}^{233}$ | $T_{10}^{323}$ | $T_{10}^{223}$ | $T_{10}^{232}$ |
| $T_{10}^{222}$ | $\frac{1}{\sqrt{3}} \Sigma^+$ | $T_{10}^{323}$ | $T_{10}^{332}$ | $T_{10}^{232}$ | $T_{10}^{322}$ |
| $T_{10}^{321}$ | $\frac{1}{\sqrt{6}} \Sigma^0$ | $T_{10}^{113}$ | $T_{10}^{131}$ | $T_{10}^{112}$ | $T_{10}^{121}$ |
| $T_{10}^{311}$ | $\frac{1}{\sqrt{6}} \Sigma^-$ | $T_{10}^{131}$ | $T_{10}^{311}$ | $T_{10}^{121}$ | $T_{10}^{211}$ |
| $T_{10}^{322}$ | $\Delta^{++}$                 | $T_{10}^{123}$ | $T_{10}^{213}$ | $T_{10}^{122}$ | $T_{10}^{212}$ |
| $T_{10}^{331}$ | $\Delta^+$                    | $T_{10}^{213}$ | $T_{10}^{231}$ | $T_{10}^{212}$ | $T_{10}^{221}$ |
| $T_{10}^{332}$ | $\frac{1}{\sqrt{3}} \Delta^0$ | $T_{10}^{231}$ | $T_{10}^{132}$ |                | $T_{10}^{221}$ |
| $T_{10}^{111}$ | $\Delta^-$                    | $T_{10}^{132}$ |                |                |                |

TABLE IX. The  $T_{10}^{ijk}$  decuplet states in SU(3).

$$B_8 = \begin{pmatrix} \frac{\Lambda}{\sqrt{6}} + \frac{\Sigma^0}{\sqrt{2}} & \Sigma^+ & p \\ \Sigma^- & -\frac{\Lambda}{\sqrt{6}} - \frac{\Sigma^0}{\sqrt{2}} & n \\ \Xi^- & \Xi^0 & \sqrt{\frac{2}{3}}\Lambda \end{pmatrix} \quad (\text{B7})$$

$$\Pi_8 = \begin{pmatrix} \pi^0 + \frac{\eta}{\sqrt{3}} & -\sqrt{2}\pi^+ & -\sqrt{2}K^+ \\ \sqrt{2}\pi^- & -\pi^0 + \frac{\eta}{\sqrt{3}} & -\sqrt{2}K^0 \\ \sqrt{2}K^- & \sqrt{2}\bar{K}^0 & -\frac{2}{\sqrt{3}}\eta \end{pmatrix} \quad (\text{B8})$$

After expanding  $\mathcal{L}_{\text{int}}^{10 \rightarrow 8 \oplus 8}$ , the Clebsch-Gordan coefficients obtained are:

$$c_{\Delta^* \rightarrow \Sigma^+ + K^0} = \sqrt{\frac{2}{3}} \quad (\text{B9})$$

$$c_{\Delta^* \rightarrow \Sigma^0 + K^+} = -\frac{2}{\sqrt{3}} \quad (\text{B10})$$

$$c_{\Delta^* \rightarrow p + \pi^0} = \frac{2}{\sqrt{3}} \quad (\text{B11})$$

$$c_{\Delta^* \rightarrow n + \pi^+} = -\sqrt{\frac{2}{3}} \quad (\text{B12})$$

The Clebsch-Gordan coefficients being equal for the  $\Delta^* \rightarrow \Sigma^0 + K^+$  and  $\Delta^* \rightarrow p + \pi^0$  decays (vis. a sign difference), the corresponding relative decay width ratios will differ only by the relative center-of-mass momentum between the  $K^+$  and  $\pi^0$ , modulo the  $2l + 1$  power from the angular momentum:

$$\frac{\Gamma_{\Delta(1900) \rightarrow \Sigma^0 + K^+}}{\Gamma_{\Delta(1900) \rightarrow p + \pi^0}} = \frac{|\mathbf{P}_{K^+}|}{|\mathbf{P}_{\pi^0}|} \quad (\text{B13})$$

$$\frac{\Gamma_{\Delta(1910) \rightarrow \Sigma^0 + K^+}}{\Gamma_{\Delta(1910) \rightarrow p + \pi^0}} = \left[ \frac{|\mathbf{P}_{K^+}|}{|\mathbf{P}_{\pi^0}|} \right]^3 \quad (\text{B14})$$

$$\frac{\Gamma_{\Delta(1920) \rightarrow \Sigma^0 + K^+}}{\Gamma_{\Delta(1920) \rightarrow p + \pi^0}} = \left[ \frac{|\mathbf{P}_{K^+}|}{|\mathbf{P}_{\pi^0}|} \right]^3 \quad (\text{B15})$$

- [1] H. Arenhövel and M. Sanzone, *Few-Body Syst. Suppl.*, **3** (1991).
- [2] I. Niculescu *PhD thesis*, Hampton University (1999).
- [3] V. Frolov *et al.*, *Phys. Rev. Lett.*, **82**: (1999).
- [4] C. Armstrong *PhD thesis*, Univeristy of William and Mary (1999).
- [5] D. J. Candlin *et al.*, Rutherford Appleton Laboratory preprint, (Sept. 1983).
- [6] J. F. David, *PhD thesis*, CEA Saclay (1995).
- [7] J. Reinhold *et al.*, *Nucl. Physics*, **A639**, 197c (1998).
- [8] G. Niculescu *et al.*, *Nucl. Physics*, **A639**, 189c (1998).
- [9] R. Mohring, *PhD thesis*, Univeristy of Maryland (1999).
- [10] D. Koltenuk, *PhD thesis*, Univeristy of Pennsylvania (1999).
- [11] J. Cha, *PhD thesis*, Hampton Univeristy (1999).
- [12] R. Williams, *PhD thesis*, North Carolina State Univeristy (1993).
- [13] N. Isgur, *Nucl. Phys.*, **B243**, 189 (1984).
- [14] Y. Nambu, *Dynamical Symmetries and Fundamental Fields*, in B. Kursunoglu, A. Perlmutter and A. Sakmar, *Symmetry Principles at High Energies*, 2nd Coral Gables Conference, p.274-85 (1965).
- [15] H. Lipkin, *Phys. Lett.*, **B195**, 484 (1987).
- [16] C. Guignoux, *Phys. Lett.*, **B193**, 323 (1987).
- [17] H. Lipkin, In Proceedings of the Rheinfels Workshop 1990 on Hadron Mass Spectrum, St. Goar at the Rhine, Germany, (1990), *Nucl Phys.*, **21B** (Proc. Suppl.), 258 (1991).
- [18] S. May-Tal Beck, In Proceedings of the 1994 Annual Meeting of the Division of Particles and Fields, Albuquerque, N. M., S. Seidel, Ed., World Scientific, 1177 (1995).
- [19] R. L. Jaffe, *Phys. Rev. Lett.*, **38**, 195 (1977).
- [20] J. L. Rosner, *Phys. Rev.*, **D33**, 2043 (1986).
- [21] P. McKenzie and H. Thacker, *Phys. Rev. Lett.*, **65**, 2539 (1985).
- [22] I. Wetzorke99, *et al.*, *e-print hep-ph/990903* (1999).
- [23] B. Nicolescu, J. M. Richard, and R. Vinh Mau, *Proceedings of the Workshop on Baryonium and Other Unusual Hadron States*, Institut de Physique Nucléaire, Orsay, France (1979).
- [24] Particle Data Book, *Phys. Rev.*, **D45**, part II, p.VIII.58 (1992).
- [25] J. Weinstein and N. Isgur, *Phys. Rev. Lett.*, **48** (1982); *Phys. Rev.*, **D27**, 588 (1983).
- [26] Y. Ho, B. Y. Park and D. P. Min, *Phys. Lett.*, **B**, 331 (1994).
- [27] D. V. Vavilov *et al.*, *Yad. Fiz.*, **57**, 241 (1994)S; V. Golovkin *et al.*, *Z. Phys.*, **C68**, 585 (1995).
- [28] L. G. Landsberg (SPHINX Collaboration), in *Proceedings of the 14th Conference on Particles and Nuclei*, edited by Carl E. Carlson and John J. Domingo, World Scientific, Singapore, 530 (1997).
- [29] C. Bennhold *et al.*, *e-print nucl-th/9909022* (1999).
- [30] SAPHIR collaboration, M. Bockhorst *et al.*, *Z. Phys.*, **C63**, 37 (1994); C. Benhold *et al.*, *Nucl. Phys.*, **A639** (1998).
- [31] G. Niculescu *et al.*, *Phys. Rev. Lett.*, **81**, 1805 (1998).
- [32] W. Roberts and S. Capstick, *Phys. Rev.*, **D49**, 4570 (1994); and *Phys. Rev.*, **D58**, 074011 (1998).
- [33] B. Saghai *et al.*, *Hypernuclear Physics with Electromagnetic probes (HYPJLAB99) workshop*, Hampton, Virginia (1999).
- [34] B. S. Han *et al.*, *e-print nucl-th/9912011* (1999).
- [35] S. Godfrey and N. Isgur, *Phys. Rev.*, **D32**, 189 (1985); S. Capstick and N. Isgur, *Phys. Rev.*, **D34**, 2809 (1986).
- [36] L. Ya. Glozman *et al.*, *e-print hep-ph/9706507* (1997); and *Phys. Rev.*, **C57**, 3406 (1998).
- [37] CEBAF Large Acceptance Spectrometer (CLAS)  $N^*$  program at Jefferson Lab. Proceedings of the PANIC99 conference, Upsala, Sweden (1999).
- [38] T. Feuster and U. Mosel, *Phys. Rev.*, **C58**, 457 (1998).
- [39] N. Mukhopadhyay, in *Proceedings of the Excited Baryons 1988 Conference*, edited by G. Adams, N. Mukhopadhyay and P. Stoler, World Scientific, Rensselaer Polytechnic Institute, 205 (1988).
- [40] A. DeRújula, H. Georgi and S. L. Glashow, *Phys. Rev.*, **D12**, 147 (1975).
- [41] CLAS collaboration, Jefferson Lab (1999).
- [42] M. de Crombrughe, H. Högaasen and P. Sorba, *Nucl. Phys.*, **B156**, 347 (1979).
- [43] H. Högaasen and P. Sorba, *Nucl. Phys.*, **B145**, 347 (1978).
- [44] A. Chodos, R. L. Jaffe, K. Johnson, C. B. Thorn and V. F. Weisskopf, *Phys. Rev.*, **D9** (1974).
- [45] K. Johnson and C. Thorn, *Nucl. Phys.*, **B41**, 397 (1978).
- [46] M. Vanderhaeghen *et al.*, *Phys. Rev.*, **C57**, 1454 (1998); M. Guidal *et al.*, *Nucl. Phys.*, **A627**, 645 (1997).
- [47] M. Guidal, J. M. Laget and M. Vanderhaeghen, *e-print hep-ph/9904511* (1999).
- [48] J. Weinstein and N. Isgur, *Phys. Rev.*, **D41**, 2236 (1990).

- [49] R. A. Schumacher, *Phys. Rev.*, **C56**, 2774 (1997).
- [50] T. Barnes and E. Swanson, *Phys. Rev.*, **C49**, 1166 (1994).
- [51] R. L. Jaffe, *Phys. Rev.*, **D15**, 267 (1977).
- [52] E. Swanson, private communication (1999).
- [53] M. Vanderhaeghen, private communication (1999).
- [54] Jefferson Lab Lattice Collaboration Group, private communication (1999).
- [55] *Phys. rev.*, *C*, Full listing (1998).
- [56] O. K. Baker *et al.*, CEBAF Proposal PR93-018.
- [57] B. Zeidman *et al.*, CEBAF Proposal PR91-016; Experiment E91-016 (phase I completed in Fall 1996).
- [58] Conceptual Design Report, CEBAF (1990).
- [59] P. Guèye *et al.*, *Monte Carlo Simulation For The  $p(\bar{e}, e'K)\bar{\Lambda}$  Reaction*, Jefferson Lab Internal Report (1999).
- [60] M. Berz, COSY INFINITY, User's Guide and Reference Manual, (1995).
- [61] G.F. Chew, M. Goldberger, F.E. Low, and Y. Nambu, *Phys. Rev.*, **106**, 1345 (1957).
- [62] R.A. Williams and T.M. Small, *Phys. Rev.*, **C55**, 882 (1997).
- [63] I.S. Barker, A. Donnachie, and J.K. Storrow, *Nucl. Phys.*, **B95**, 347 (1975).
- [64] C.G. Fasano, F. Tabakin, and B. Saghai, *Phys. Rev.*, **C46**, 2438 (1992).
- [65] G. Knochlein *et al.*, *Z. Phys.*, **352**, 327-943 (1995).
- [66] E. Amaldi, S. Fubini, G. Furlan, Pion Electro-production, Berlin, Springer (1979).